Zeitschrift: IABSE reports = Rapports AIPC = IVBH Berichte
Band: 999 (1997)

Rubrik: Behaviour modelling

Plastic Deformation Capacity of Steel-Concrete Composite Member

Toshiro SUZUKI
Prof. Emeritus, Dr. Eng.
Tokyo Institute of Technology
Tokyo, JAPAN

Shojiro MOTOYUI
Assoc. Prof., Dr. Eng.
Tokyo Institute of Technology
Yokohama, JAPAN

Takashi FUKASAWA
Manager, Dr. Eng.
Tomoe Corporation
Tokyo, JAPAN

Masahiko UCHIYAMA
Civil Engineer, Dr. Eng.
Tomoe Corporation
Tokyo, JAPAN

Summary

Various attempts have recently been undertaken to improve plastic deformation capacity of steel members. One of these is the approach of combining with concrete as the composite member. In respect to the composite beam-column which is made of H-shaped steel and concrete placed between upper and lower flange of the steel, the present paper describes quantitative evaluation of stiffening effect by concrete and also quantitative evaluation of plastic deformation capacity of the proposed structural configuration.

1. Introduction

Steel-concrete composite is conventionally considered as a steel encased by the reinforced concrete in Japan. The structural portion outside the steel in the composite is significant for strength of the member. However, such the composite is especially difficult to improve its plastic deformation until the load carrying capacity, because the load carrying capacity is dominated by crush of the concrete. Therefore, to investigate concrete stiffening effect to the steel, the objective in the present study is H-shaped section of the steel filled by concrete between the both flange plates, which is hereafter called SC. In this paper, firstly local buckling behavior and collapse mechanism of SC is discussed, secondary the specific criterion of the collapse is derived theoretically, and then method of evaluating the plastic deformation capacity is proposed.

2. Modelling of Local Buckling Behavior

2.1 Experimental Approach

Several kinds of tests[1),2),3),4)] have been carried out on the proposed structural configuration shown as cross-section in Fig. 1. Regarding effect of concrete, the most typical results have been obtained also by a test of cyclic flexural loading, noticed as Q in Fig. 1, under keeping a constant axial force, noticed as N. Two types of specimens, shown in Fig. 1, have been tested to clarify effect of concrete. One of these described as type SC is the objective in case that concrete is undergoing axial force. The other, type SC-s, is the objective in case that concrete is not affected by the applied axial force, which is realized by several urethane plates inserted in concrete as shown in Fig. 1. Used material combination is fixed to SM490A of steel, of which tensile yield stress is over 324N/mm^2 regulated by Japan Industrial code, and concrete required

34N/mm^2 of compressive strength.
Experimental results[4] of using a fixed size of steel, BC2 in Table 1, are shown in Fig. 2, comparing load versus displacement relation of the type of SC and SC-s with that of the only steel. Sufficient concrete stiffening effect to the steel in the composite is admitted by hysteresis characteristics of type SC or type SC-s. Specimen of the only steel is observed instability at the end of the first cycle according to forming local shear buckling of web plate, represented in Photo. 1(c). However, local buckling mode of the type of SC or SC-s is different from that of the steel, which is web plate stretched normal to the axial direction without out-of-plane deformation. Therefore, the concrete is considered to stiffen web plate. Some of the other experimental results are given in Table 1, which consists also results[3),4)] of monotonously flexural loading without axial force. The plastic deformation capacity of SC is determined to be much higher than that of the only steel.

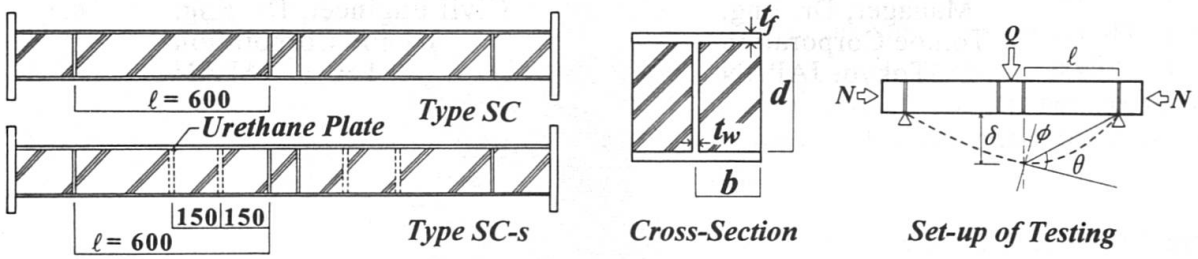

Fig. 1 Schematic of Specimens

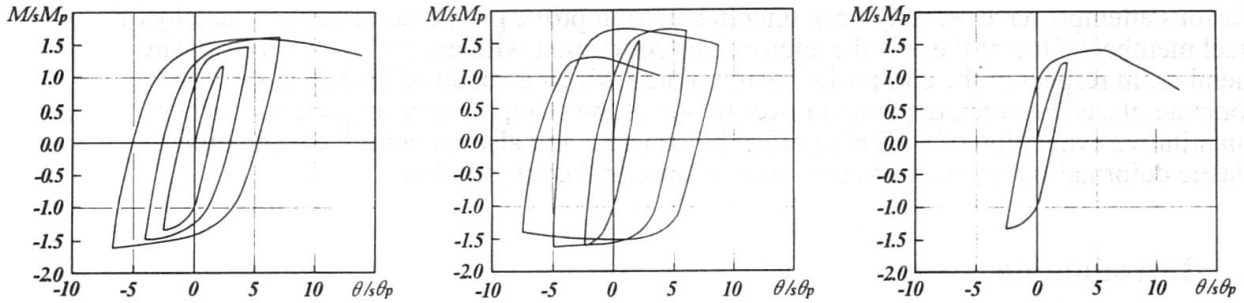

(a) Type SC(BC2) (b) Type SC-s(BC2-s) (c) Steel

Fig. 2 Concrete Stiffening Effect to Steel Member

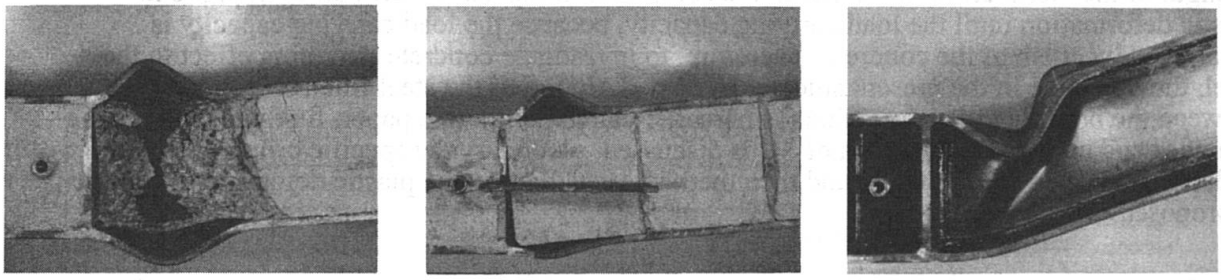

(a) Type SC(BC2) (b) Type SC-s(BC2-s) (c) Steel

Photo. 1 Close-up of Local Buckling after Failure

Table 1 Experimental Results

Cyclic flexural loading with axial force:

Specimen	b/t_f	d/t_w	N_u (kN)	n'	M_m(kN·m)	R
BC1	16.7	31.3	1450	0.3	6.7	3
BC2	8.33	29.3	1870	0.3	10.8	10
BC3	8.33	22.0	1930	0.3	10.7	20

Monotonously flexural loading without axial force:

Specimen	b/t_f	d/t_w	M_m(kN·m)	R
B1	16.7	31.3	6.8	10
B2	12.5	30.7	8.8	14
B3	12.5	23.0	9.2	14

Note: N_u is the calculated compressive strength of the composite, but N_u of BC2-s(type SC-s) is for only steel., n' is ratio of the applied axial force to N_u., M_m is moment at the max. load., R: is plastic deformation capacity defined by plastic deformation at the load carrying capacity.

2.2 Numerical Approach

The particular local buckling mode, described in the former, is considered to be significant for evaluating plastic deformation capacity of SC. Therefore, compressive tests[2] on stub columns have been carried out to investigate the buckling behavior. After failure web plate was observed to be stretched normal to the axial direction, but it was not deformed out-of-plane. Considering this phenomenon, the numerical analysis by finite element method has executed under the following boundary condition: out-of-plane displacement of web plate is constrained, and the other boundaries are governed by the same condition of the steel. In order to focus concrete stiffening effect, bearing load by concrete should be eliminated. Therefore, in this stub column test, specimens of SC are fixed to type SC-s, and the analytical model is subjected to a steel member without concrete. With respect to load-displacement characteristic and deformation after failure, the each analytical result is corresponding to the experimental result, which is shown in Fig. 3. Consequently, the present analytical model is verified by these results.

Several cases are analyzed numerically by the proposed model as a parameter of width-to-thickness ratio of web plate under that of flange plate fixed to 7.29. In these analytical results shown in Fig. 4, displacements at two points in the section of flange plate, noticed as w_1 and w_2, are discussed. If the buckling criterion of flange plate, noticed as ▽, is defined w_1 becomes 15% of flange plate thickness, the each point of this criterion in the load-displacement curve is determined to be shifted to that of infinite small width-to-thickness ratio of web plate in an asymptotic manner. Moreover, the each point of the load carrying capacity is determined to be located far from the point of the buckling criterion. Therefore, collapse mode should be affected by some other except buckling of flange plate. On the other hand, the provisional collapse criterion noticed as ▲ which is defined that displacement w_2 becomes 2% of width of flange plate. The each point of this collapse criterion is located after the point of the buckling criterion and nearer to the each point of the load carrying capacity. Therefore, collapse mode should be affected by stretching of web plate normal to the axial direction. Moreover, behavior of flange plate is mentioned to be similar to buckling of a lateral stiffened simple column shown in Fig.5.

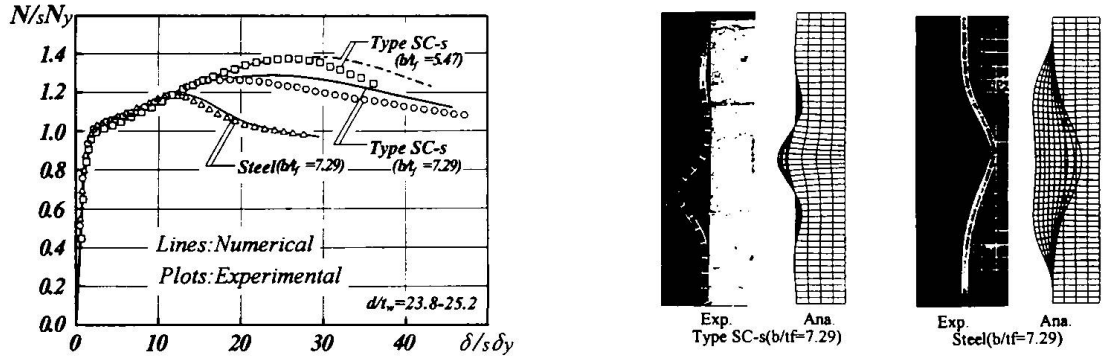

(a) Load-displacement Characteristics (b) Deformation after Failure

Fig. 3 Verification of Analysis

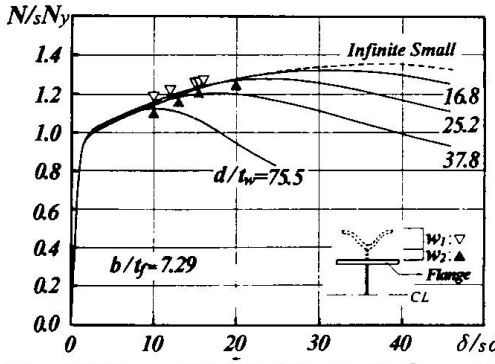

Fig. 4 Effect of Web to Plastic Deformation

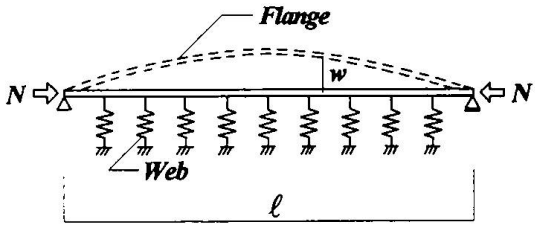

Fig. 5 Collapse Mechanical Model

2.3 Theoretical Treatment

From the above mentioned, which is significant on behavior of web plate stretching in the collapse mode, the collapse mechanism should be imagined by a model of simplified flange plate stiffened by many springs which is illustrated in Fig. 5. Collapse criterion of this model is able to be equivalent to buckling criterion of the lateral stiffened column. The bucking equation[5] of such the column is represented as eq. 1. In this equation, 'EI' is the flexural stiffness of the column which is provided with section properties of flange plate, and 'k' is the spring constant which is provided with section properties of web plate.

$$EI\frac{d^4w}{dx^4}+N\frac{d^2w}{dx^2}+kw=0 \quad \text{where,} \quad EI=\frac{Et_f^3b}{12(1-\nu^2)}, \quad k=\frac{Et_w}{(1-\nu^2)d} \qquad \cdots\cdots\cdots \text{Eq. 1}$$

The above equation can be written in the non-dimensional form represented as eq. 2. Assumed a constant compressive force applying to the section, n(ξ)=1, a solution of eq. 2 is Asin(iπξ), where 'A' is a constant number, and 'i' is the wave number. Then, 'λ' is obtained as eq. 3 in case of infinite long column. Therefore, the buckling strength N_{cr} is given by eq. 4.

$$\frac{d^4w}{d\xi^4}+\pi^2\lambda n(\xi)\frac{d^2w}{d\xi^2}+(\beta\ell)^4w=0 \qquad \cdots\cdots\cdots\cdots\cdots\cdots\cdots\cdots\cdots\cdots \text{Eq. 2}$$

$$\text{where,} \quad \xi=x/\ell,\beta=\left(\frac{k}{EI}\right)^{\frac{1}{4}},n(\xi)=N/N_e,\lambda=\frac{N_e}{N_E},N_E=\frac{\pi^2EI}{\ell^2}$$

$$\lambda=2\frac{\ell^2}{\pi^2}\sqrt{\frac{k}{EI}} \qquad \cdots\cdots\cdots \text{Eq. 3} \qquad N_{cr}=2\sqrt{\frac{E^2t_wt_f^3b}{12(1-\nu^2)^2d}} \qquad \cdots\cdots\cdots \text{Eq. 4}$$

Finally, the buckling stress is given by eq. 5. Namely, this equation is related to the generalized slenderness, therefore; a geometrical term in eq. 5 is significant to examine behavior of the collapse. To evaluate efficiency of this term which is hereafter called α represented as eq. 6, the experimental results and the analytical results have been discussed on this α. A high correlation between the load carrying capacity or the plastic deformation capacity and α is recognized as shown in Fig. 6 (a), (b) respectively. Consequently, α is considered as a criterion of the collapse.

$$\left(\frac{\sigma_y}{\sigma_{cr}}\right)^{-1}=\frac{E}{\sqrt{3}(1-\nu^2)\sigma_y}\sqrt{\left(\frac{t_w}{d}\right)\left(\frac{t_f}{b}\right)} \qquad \cdots\cdots \text{Eq. 5} \qquad \alpha=\sqrt{\left(\frac{t_w}{d}\right)\left(\frac{t_f}{b}\right)} \qquad \cdots\cdots \text{Eq. 6}$$

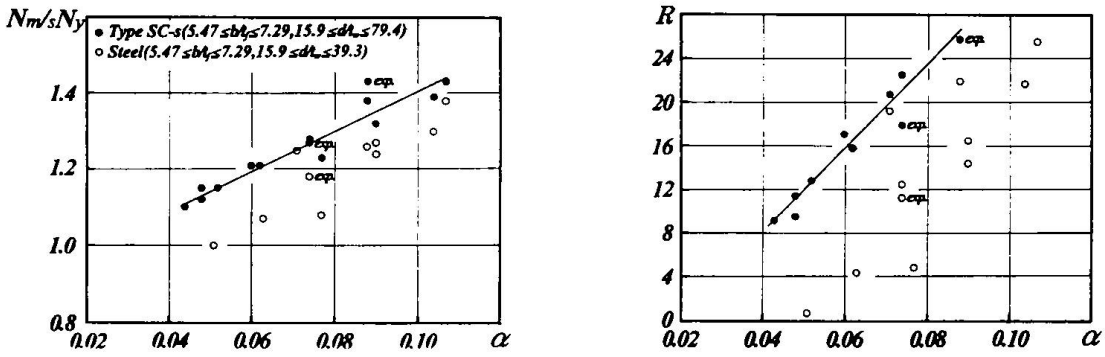

(a) Strength (b) Plastic Deformation Capacity

Fig. 6 Efficiency of Parameter α

3. Plastic Deformation Capacity

3.1 Method of Evaluating

Several assumptions and approximations are necessary to evaluate the plastic deformation capacity of the composite beam or beam-column. Firstly, it is assumed that effect of the concrete strength is ignored, because concrete in the present composite is crushed near after the yield of the steel, which is noticed as the point of 'b' in Fig. 7. Secondary, shape of the section is equivalent to the simplified model so called as the two-flange model[6], which consists only the upper and lower flange plates having the equivalent area of the original section and moment of inertia. Furthermore, according to the well known approximation for the steel, load-displacement curve of the composite is simplified to the linear model as shown in Fig. 7. On the other hand, plastic zone of the member is defined as the illustration in Fig. 8 which is the equivalent cantilever beam-column model. In this illustration, noticed 'n' means the ratio of the actually applying axial force to the steel in the composite. The actual value of this ratio can be approximately calculated according to the following assumption: The steel is assumed to be undergoing the all applied axial force between the point of 'b' and 'c' in Fig. 7. Additionally, in this model the plastic deformation capacity 'R' is defined by the equation: $R=\delta_{m2}/\delta_{m1}-1$.

Based on the model and the assumptions, distribution of the flexural moment is described as eq. 7. With respect to displacement after the point of the maximum strength of the steel noticed as 'b' in Fig. 7, relations of the moment to the curvature corresponding to the distinct loading or stress conditions are defined as eqs. 8,9,10; these equations are in case of no axial force applying, and in cases that the tensile flange plate, which is the lower flange plate, yields or keeps elastic under the applied constant axial force, respectively. The tensile flange plate tends to yield if the parameter α is relatively large; however, the present investigation does not examine the specific point of this yielding, which is considered as the future work. Finally, based on distribution of the curvature derived from these relations, the plastic deformation capacity of the each case, especially the flexural displacement at the free end in Fig. 8, is obtained by the similar process[6] for the steel. The plastic deformation capacity is consequently described as a function of the parameter α, the section properties, the material mechanical properties, and two ratios of the applied axial force to the calculated compressive strength of the steel before and after crush of the concrete.

$$M(x) = (1-n)\cdot M_{p0} + (s_2 - 1)\cdot M_{p0}\left(\frac{\tau_3 \ell - x}{\tau_3 \ell}\right) \quad \cdots\cdots \text{Eq. 7}$$

$$M = S_1 \cdot M_{p0} + D(\phi - \phi_m) \text{ , where } \quad D = \frac{(S_2 - S_1)EI}{374\alpha' - 6.93 - (S_1 - 1)(E / E_{st})} \quad \cdots\cdots \text{Eq. 8}$$

$$M = S_1 \cdot M_{p0} + D(\phi - \phi_m - \phi_u) \quad \cdots \text{Eq. 9}$$

where $\phi_u = (\varepsilon_u - \varepsilon_y)/h$

$$M = S_1 \cdot M_{p0} + 2D(\phi - \phi_m) \quad \cdots \text{Eq. 10}$$

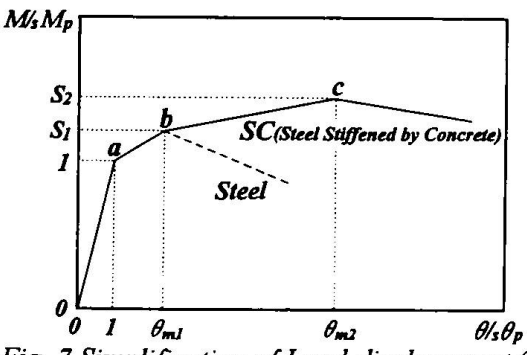

Fig. 7 Simplification of Load-displacement Curve

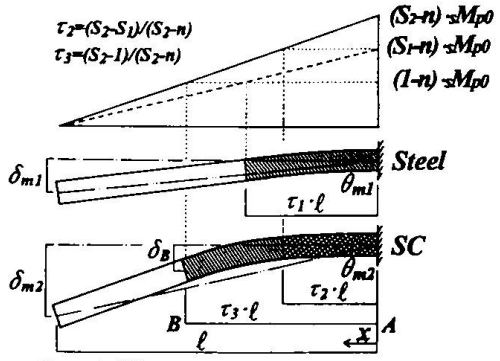

Fig. 8 Plastic Zone of Beam-column

3.2 Verification

Arranging the expression of evaluating the plastic deformation capacity 'R', almost linear correlation between 'R' and the parameter α is obtained, which is shown as lines in Fig. 9 corresponding to the distinct loading or stress condition. The proposed method of evaluating is verified by the experimental results, however in case of with axial force, two situations are considered whether the tensile flange yields or not. Transition point among these situations is not specified, but at least the equation for the tensile flange plate keeping elastic is adopted at the safety side. Furthermore, based on the relation of 'R' to α, limitations for width-to-thickness of flange and web plates are obtained as shown in Fig. 10. Consequently, these limitations of the steel in the composite is much lightened comparing with the steel only.

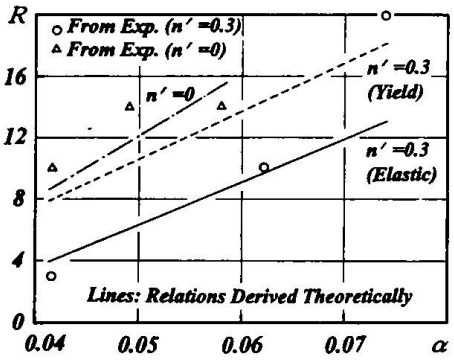

Fig. 9 Plastic Deformation Capacity

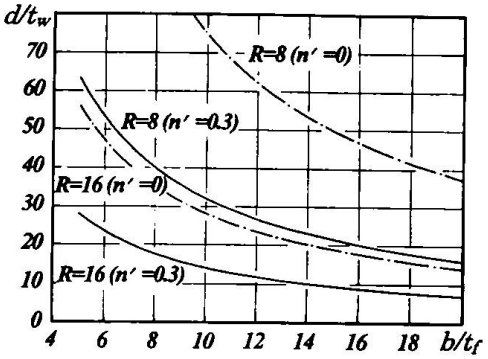

Fig. 10 Width-to-thickness Limitations

4. Conclusions and Future Works

The collapse mechanism of the proposed composite is clarified to be stretching of web plate normal to the axial direction. Theoretically derived from this mechanism, the geometrical parameter α is determined as criterion of the collapse. Furthermore, α is efficient to evaluate the plastic deformation capacity of the beam and the beam-column quantitatively. As future works, the proposed method of evaluating should be optimized to clarify the transition point of the tensile flange plate yielded. Additionally, effect of bearing ratio between the steel and the concrete should be evaluated in the proposed method.

References

1) Suzuki, T., Ogawa, T., Fukasawa, and Uchiyama, M., "An Experimental Study on Structural Properties of Steel-concrete Columns under Compressive Shear Stress"(in Japanese), J. Struct. Constr. Eng., AIJ, No. 483, pp. 165-172, May, 1996.
2) Suzuki, T., Motoyui, S., Uchiyama, M., "Study on Strength and Plastic Deformation Capacity of Composite Stub Column under Compressive Loading"(in Japanese), J. Struct. Constr. Eng., AIJ, No. 480, pp. 171-178, Feb., 1996.
3) Suzuki, T., Motoyui, S., Uchiyama, M., "Study on Plastic Deformation Capacity of Composite Member under Bending Shear Loading"(in Japanese), J. Struct. Constr. Eng., AIJ, No. 484, pp. 141-148, Jun., 1996.
4) Suzuki, T., Motoyui, S., Uchiyama, M., "Study on Plastic Deformation Capacity and Hysteresis Characteristics of Composite Member Loaded Cyclic Bending Moment under Constant Axial Loading"(in Japanese), J. Struct. Constr. Eng., AIJ, No. 490, pp. 213-220, Dec., 1996.
5) S. E. Svensson, "Lateral Buckling of Beams Analyzed as Elastically Supported Columns Subject to a Varying Axial Force", J. Constr. Steel Research, Vol.5, pp.179-193, 1985.
6) Kato, B., Nakao, M., "Strength and Deformation Capacity of H-shaped Steel Members Governed by Local Buckling"(in Japanese), J. Struct. Constr. Eng., AIJ, No. 458, pp. 127-136, Apr., 1994.

The Fracture Theory of Composite at Bearing Strain in End Faces

A.N. GUZ
Prof., Director
Institute of Mechanics
Kiev, Ukraine

A.N. Guz, born 1939, member of the Academia European the National Academy of Sciences of Ukraine and the New York Academy Sciences, published 44 monographs and about 700 scientific papers, supervisor of 30 doctor of Sciences and 90 candidate of Sciences dissertations.

Summary

In continual approximation for construction of the theory of fracture the material is modelled by orthotropic elastic (in case of brittle fracture) or by elastic–plastic (in case of plastic failure) body. For modelling of the fracture mechanism considered the phenomenon of surface instability near the end face is used. The exact solution was used for computation of theoretical strength limits, corresponding to fracture at bearing strains on end faces. The comparison with experimental results was made for unidirectional fibrous materials.

1. Introduction

The article is devoted to investigation of mechanism of fracture of composite materials and of structures elements fabricated from these materials in compression, when in end faces bearing strains occur. This phenomenon occurs, for example, in uniaxial compression when fracture of material initiates near end faces. This fracture is not propagated far from end faces. For this reason, the ultimate strength of material, corresponding to fracture at bearing strains in end faces, is some what lower than the ultimate strength of the material at the fracture of the whole material (far from end faces). For description of this phenomenon the continual theory of fracture is proposed with modelling of material (in continual approximation) by orthotropic elastic (in case of brittle fracture) or by elastic–plastic (in case of plastic failure) body. The phenomenon of surface instability is applied for modelling the fracture mechanism considered. For description of phenomenon of surface instability under applied normal load the three–dimensional linearized theory of deformable bodies stability, which is presented, for an example, in [2] is used. For solution of formulated problems (within the framework of linearized theory of deformable bodies stability) the system of integral representations is used. As a result of exact solution equations are obtained for determination of theoretical values of ultimate strength related to fracture at bearing strains in end faces. Values of theoretical ultimate strength are computed related to fracture at bearing strains in end faces with application of composite materials with polymer (brittle fracture) and metal (plastic failure) matrix. Comparison was made with results of experimental studies for unidirectional fibrous composites.

2. Main relations and statements

Fracture at bearing strains in end faces occurs under compression. It consists of local fracture near end faces. When the increase of compressive load is insignificant no propagation of fracture far from end faces occurs. This fracture mechanism is realized also in structural elements fabricated from composite materials in places where they are joined with metal structural elements. The fracture at bearing strains is very marked in case of unidirectional fibrous composite under compression along the fibers and the layers, when the end faces are not fixed by special procedures. Consequently, following special features are characteristic of fracture mechanism at bearing strains in end faces.

1. It occurs mainly under compression of unidirectional fibrous composites and of laminated composites (under compression along fibers and layers).
2. It occurs mainly in cases with unfixed end faces.
3. It occurs near end faces and does not propagate far from end faces.

For an example we consider the unidirectional fibrous boron–aluminium in the case of 50% content of the fibers under uniaxial compression along the fibers. Nature of fracture at bearing strain in end face of this composite is shown on Fig.1. Since the compression along fibers or layers and end faces is analysed, it is logical to assume that at the initial stage a local stability loss occurs (the surface instability near the loaded end face). The foregoing considerations lead to following main statements of the present continual theory.

1. In the analysis of the phenomenon of bearing strains in end faces the influence of lateral surface of the specimen or of the structural element will be not accounted for. This statement allows to analyse the lower half–space ($x_3 = 0$).
2. The phenomenon of bearing strain in end faces at the initial stage will be assumed to occur as a result of surface stability loss near the loaded end face. Only surface instability will be analysed, when stresses and displacements attenuate at increasing distance from the end face.

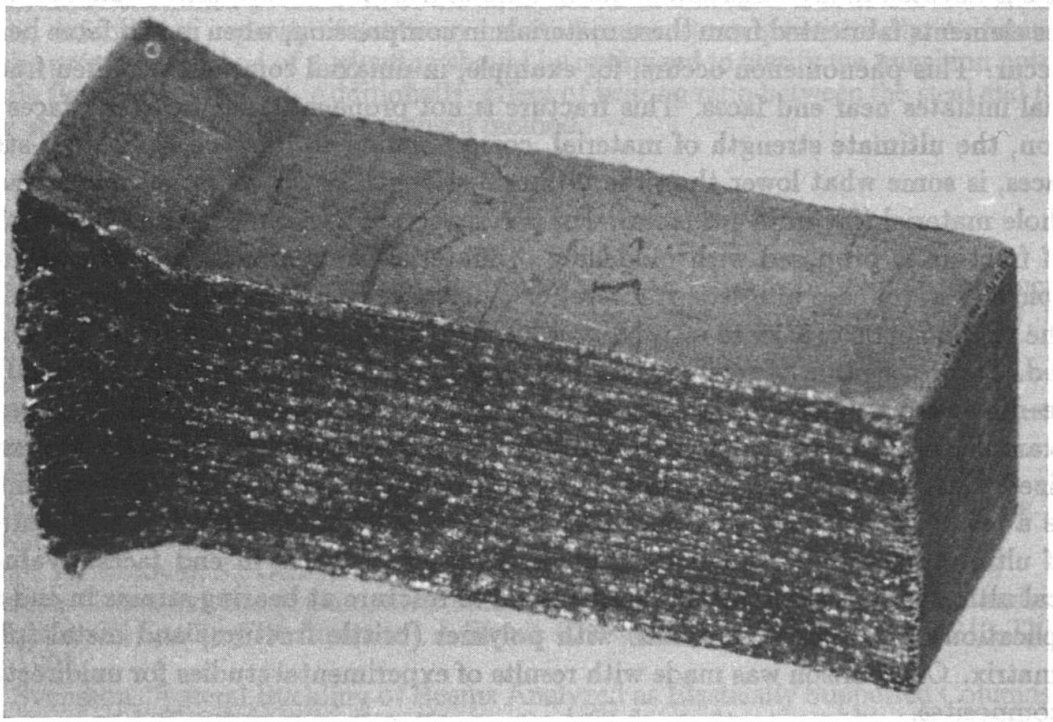

Fig.1. Fracture of unidirectional composite at bearing strains in end face in axial compression (boron–fibers, aluminium–matrix). The view after fracture

3. The analysis of surface instability near the loaded end face will be carried out within the framework of the three–dimensional linearized theory of deformable bodies stability [1,2]. The second variant of the small practical deformations theory will be used [2] (precritical state is determined with the use of geometrically linear theory).
4. In the analysis of plastic failure (materials with metal matrix) the generalized conception of continuing loading will be used [1,2]. Consequently, we will not take account of the change of unloading zones in the process of stability loss. This statement allows to analyse in the general form the brittle and plastic failure.
5. The precritical state will be assumed to be homogeneous in the analysis of surface instability near the loaded end face.
6. The external load at $x_3 = 0$ will be assumed "dead" load, and this validates the use of static method of analysis [2].

7. Laminated and fibrous composites will be considered. For laminated composites it will be assumed that layers are directed perpendicularly to the end face surface $x_3 = 0$. With application to fibrous composites the unidirectional or orthogonally reinforced materials will be analysed under the condition that the direction of main reinforcement is perpendicular to the end face $x_3 = 0$.
8. In continual approximation these composites will be modelled by compressible homogeneous orthotropic body. The model will be used of elastic linear body at brittle fracture (in case of polymer matrix) and the model of elastic–plastic body at plastic failure (in case of metal matrix). The assumption will be made that the axes of symmetry of material properties (in continual approximation) coincide with axes of the chosen coordinate system. In case of the model of transversely isotropic body the planes $x_3 = const$ will be assumed as isotropy planes.
Taking into account the foregoing main statements we will consider main relations. For three–dimensional precritical state main equations of the three–dimensional linearized theory of deformable bodies stability [2] with application to compressible bodies have the form

$$L_{m\alpha}u_\alpha = 0; \qquad n, m, \alpha, \beta = 1, 2, 3;$$
$$L_{m\alpha} = \omega_{nm\alpha\beta}\frac{\partial^2}{\partial x_n \partial x_\beta}; \qquad \omega_{nm\alpha\beta} = \omega_{nm\alpha\beta}(\sigma^0_{11}, \sigma^0_{22}, \sigma^0_{33}) \tag{2.1}$$

Components of the asymmetric tensor of stresses of Kirchhoff are determined [2] from the expression

$$t_{nm} = \omega_{nm\alpha\beta}\frac{\partial u_\alpha}{\partial x_\beta} \tag{2.2}$$

For homogeneous precriticall state (with application to the second variant of the small precritical deformations theory [2]) following relations hold

$$\omega_{nm\alpha\beta} = \delta_{nm}\delta_{\alpha\beta}A_{n\beta} + (1 - \delta_{nm})(\delta_{n\alpha}\delta_{m\beta} + \delta_{n\beta}\delta_{m\alpha})\mu_{nm} + \delta_{n\beta}\delta_{m\alpha}\sigma^0_{\beta\beta} \tag{2.3}$$

In [2] expressions are presented for determination of values of $A_{n\beta}$ and μ_{nm} for various models. In case of brittle fracture (polymer matrix) it may be assumed

$$A_{n\beta}, \mu_{nm} = const; \qquad \mu_{nm} = G_{nm} \tag{2.4}$$

In case of plastic failure (metal matrix) it may also be assumed

$$A_{n\beta} = A_{n\beta}(\sigma^0_{11}, \sigma^0_{22}, \sigma^0_{33}) \qquad \mu_{nm} = \mu_{nm}(\sigma^0_{11}, \sigma^0_{22}, \sigma^0_{33}) \tag{2.5}$$

The existence of relations (2.5) complicates the analysis significantly.
On the end face ($x_3 = 0$) the following boundary conditions hold

$$t_{3m} = 0 \qquad \text{at} \qquad x_3 = 0; \qquad m = 1, 2, 3 \tag{2.6}$$

In view of the local character of the surface instability, the conditions of attenuation "at infinity" (at $x_3 \to -\infty$) should be put in the following form

$$u_m \to 0, \qquad t_{nm} \to 0 \qquad \text{at} \qquad x_3 \to -\infty \tag{2.7}$$

The formulation of the problems is complete with foregoing relations and with taking account of symmetry properties for components $\omega_{nm\alpha\beta}$ [2]. Consequently, the problem of eigenvalues is obtained (relative to loading parameter σ_{33}^0) in the form (2.1)–(2.7).

3. Theoretical results

Within the framework of the foregoing formulation we will consider now the computation of the theoretical strength limit corresponding to fracture at bearing strains in end faces. We will consider arbitrary form of stability loss in variables x_1 and x_2, including local (in x_1 and x_2) forms of stability loss. It should be remarked that in [2] surface instability was considered when the load was applied along the plane boundary ($\sigma_{33}^0 = 0$) and only periodical (in x_1 and x_2) forms of stability loss were investigated. In case of arbitrary forms of stability loss the solution will be represented in the form of Fourier integrals

$$u_n = \frac{1}{2\pi}\int\limits_{-\infty}^{+\infty}\int v_n(x_3,\alpha_1,\alpha_2)\{\exp[-i(\alpha_1 x_1+\alpha_2 x_2)]\}d\alpha_1 d\alpha_2;$$

$$t_{nm} = \frac{1}{2\pi}\int\limits_{-\infty}^{+\infty}\int r_{nm}(x_3,\alpha_1,\alpha_2)\{\exp[-i(\alpha_1 x_1+\alpha_2 x_2)]\}d\alpha_1 d\alpha_2; \tag{3.1}$$

Introducing (3.1) into (2.1)–(2.7) we obtain the eigenvalues problem, formulated relative to functions v_n and r_{nm} (3.1). The solution of this eigenvalues problem will not be presented here as the extent of the article is restricted, additional information may be found in [3,4]. Here only final expressions will be presented, obtained by exact solution of this eigenvalues problem. In the exact solution characteristic equations are obtained corresponding to surface instability near the loaded end face. These expressions will be presented separately for the plane and the three–dimensional problems.

In the case of the plane problem (plane deformation in the plane x_1ox_3) with application to the model of orthotropic body characteristic equations are obtained in the following form

$$\omega_{1111} = 0; \qquad \omega_{1331} = 0; \qquad \omega_{1133} + \omega_{1313} = 0; \qquad \Pi = 0 \tag{3.2}$$

In the case of three–dimensional problem (with additional condition $\sigma_{11}^0 = \sigma_{22}^0$) with application to the model of transversely isotropic body (the axis ox_3 is the isotropy axis) characteristic equations have the form

$$\omega_{3333} = 0; \qquad \omega_{3113} = 0; \qquad (\omega_{1133} + \omega_{1313})^{-1} = 0; \qquad \Pi = 0 \tag{3.3}$$

In (3.2) and (3.3) the notation is introduced

$$\Pi \equiv \sqrt{\omega_{1111}\omega_{3333}}(\omega_{3113}\omega_{1331} - \omega_{1313}^2) + \sqrt{\omega_{1331}\omega_{3113}}(\omega_{1111}\omega_{3333} - \omega_{1133}^2) \tag{3.4}$$

It should be pointed out that characteristic equations (3.2) and (3.3) taking into account the notation (3.4) are obtained in the unified general form for the finite precritical deformations theory [2] and for two variants of the small precritical deformations theory [2] in the case of elastic and elastic–plastic models. For derivation from (3.2)–(3.4) of results corresponding to the second variant of the amsll precritical deformations theory [2] (this problem is considered in this article) it is necessary to use for determination of components of the tensor ω the expressions (2.3).

In the following only the case of uniaxial compression along the axis ox_3 will be considered. In view of this the following condition should be assumed

$$\sigma_{11}^0 \equiv \sigma_{22}^0 = 0 \tag{3.5}$$

We also introduce the following notations:

$(\Pi_3^-)_{\mathrm{T}}$ – theoretical strength limit in compression along the axis ox_3, corresponding to the fracture of the whole specimen or structural element;

$(\Pi_3^-)_{\mathrm{T}}^{SM}$ – theoretical strength limit in compression along the axis ox_3, corresponding to the

fracture of the specimen or structural element at bearing strain in end face;
$(\Pi_3^-)_{ex}$ – experimental value of the strength limit in compression along the axis ox_3, corresponding to the fracture of the whole specimen or structural element;
$(\Pi_3^-)_{ex}^{SM}$ – experimental value of the strength limit in compression along the axis ox_3, corresponding to the fracture of the specimen or structural element at bearing strain in end face;
$-(\sigma_{33}^0)_{cr}$ – critical value of the compressive load, corresponding to the internal [2] stability loss in the structure (for the whole specimen, corresponding to the infinite body);
$-(\sigma_{33}^0)_{cr}^{SM}$ – critical value of the compressive load, corresponding to the local stability loss near the loaded end face.
Taking into account the foregoing notations and the second main statement of the present theory the following equality may be written

$$(\Pi_3^-)_T^{SM} = -(\sigma_{33}^0)_{cr}^{SM} \tag{3.6}$$

In analogous manner [5] we may also write

$$(\Pi_3^-)_T = -(\sigma_{33}^0)_{cr} \tag{3.7}$$

Omitting all intermediate calculations, we will present only final results concerning the evaluation of the considered theoretical strength limits. We remark that for analysed composite materials (Fig.3 and 4), taking into account the notations (2.2) and (2.3) following inequalities are valid

$$A_{33} >> G_{13}; \qquad A_{33} >> \mu_{13} \tag{3.8}$$

with application to the brittle and plastic fracture.
Taking into account (3.8) with application to the case (3.5), from (3.2)–(3.4) after some cumbersome transformations the following result is obtained

$$[(\Pi_3^-)_T - (\Pi_3^-)_T^{SM}] \cdot [(\Pi_3^-)_T]^{-1} \approx (\tfrac{\mu_{13}}{A_{33}})^2 \tfrac{A_{33}}{A_{11}} [1 - \tfrac{A_{13}^2}{A_{11}A_{33}}]^{-1} > 0 \tag{3.9}$$

For case of brittle fracture in (3.9) the value μ_{13} should be substituted for G_{13}. In view of inequalities (3.8) for structural materials the following result is obtained

$$(\Pi_3^-)_T^{SM} < (\Pi_3^-)_T \tag{3.10}$$

It means that the values of theoretical strength limits $(\Pi_3^-)_T$ and $(\Pi_3^-)_T^{SM}$ differ insignificantly.
As an example, the laminated composite at brittle fracture will be considered. We introduce notations: E_a, ν_a and S_a – Young modulus, Poisson coefficient and concentration of the filler (or reinforcing elements); E_m, ν_m and S_m – Young modulus, Poisson coefficient and concentration of the binder (of matrix). For structural materials we assume also

$$S_a \approx S_m; \qquad E_a >> E_m \tag{3.11}$$

In this case, taking into account known results, from (2.9) for a laminated composite we obtain

$$[(\Pi_3^-)_T - (\Pi_3^-)_T^{SM}] \cdot [(\Pi_3^-)_T]^{-1} \approx \tfrac{1}{4(1+\nu_m)^2} \tfrac{1}{S_a S_m} \tfrac{E_m}{E_a} \tag{3.12}$$

From (3.12), which corresponds to the considered example, it follows that the difference between theoretical strength limits $(\Pi_3^-)_T$ and $(\Pi_3^-)_T^{SM}$ is insignificant.

4. Comparison with experimental results

Three results will be considered in this chapter which related with experiments. In our comparison of theoretical results with experimental results we will use the relation (3.10), since in experimental studies quite frequency the values of $(\Pi_3^-)_T$ and $(\Pi_3^-)_T^{SM}$ are not distingwished. Values of theoretical strength limits $(\Pi_3^-)_T$ are computed in [5] for some materials.
1. Nature of fracture of unidirectional composite at bearing strains in end face in axial compression (boron–fibers, aluminium–matrix) is shown on Fig.1. The photograph of Fig.1 correspond to the view of specimen after fracture. The above mentioned fracture arose near

first end of specimen. Design and technological technigues, excluding occurence of the above mentioned fracture near second end of specimen were utilized.

2. We consider unidirectional fibrous boron–reinforced plastic in case of brittle fracture at 50% content of fibers ($S_a = S_m = 0.5$). In this case following results were obtained

$$(\Pi_3^-)_{ex} = 3.10 GPa; \qquad (\Pi_3^-)_T = 2.00 - 3.00 GPa \tag{4.1}$$

In (4.1) in determination of $(\Pi_3^-)_T$ the scatter of properties of epoxy resin is taken account of.

3. We consider the unidirectional fibrous boron–aluminium at plastic failure in the case of 50% content of fibers ($S_a = S_m = 0.5$). Results were obtained [4,5] for annealed and non–annealed aluminium, we present the results in the Table

Material	$(\Pi_3^-)_{ex}^{SM}$, MPa	$(\Pi_3^-)_T^{SM}$, MPa
annealed	665	736
non–annealed	1282	1467

These results taking into account the inequality (3.10) demonstrate a good agreement between theoretical and experimental results. Additional information and analysis of related problems are presented in monograph [5] and article [6].

References

1. Guz', A.N., "Stability of three–dimensional deformable bodies", Naukova Dumka, Kiev 1971, 272p (In Russian).

2. Guz', A.N., "Foundations of three–dimensional theory of deformable bodies stability", Vyshcha Shkola, Kiev, 1986, 512 p. (In Russian).

3. Guz', A.N., "Continual theory of fracture of composite materials at bearing strain in end faces (brittle fracture)". Prikladnaya Mekhanika, 1987, 23, N 2, pp.59–69. (In Russian).

4. Guz', A.N., "Continual theory of fracture of composite materials at bearing strains in end faces (plastic failure)". Prikladnaya Mekhanika, 1987, 23, N 5, pp.3–9. (In Russian).

5. Guz', A.N., "Mechanics of fracture of composite materials in compression", Naukova Dumka, Kiev, 1990, 630 p. (In Russian).

6. Guz', A.N., "Fracture of fibrous composites at bearing strain in end faces in compression". In: Proceedings of the Ninth International Conference on Composite Materials (ICCM/9), Madrid, 1993, v.6. Composites Properties and Applications. Pp.613–618.

Behaviour of High-strength Composite Columns

Andrew KILPATRICK
Senior Lecturer in Civil Engineering
University of Southern Queensland
Toowoomba, Qld, 4350 AUSTRALIA

Andrew Kilpatrick received his BEng degree from the CIAE in 1974, MEngSc degree from the University of Queensland in 1985 and PhD degree from Curtin University in 1997.

B Vijaya RANGAN
Professor and Head of Civil Engineering
Curtin University of Technology
Perth, WA, 6001 AUSTRALIA

Vijaya Rangan received his BE degree from Madras University in 1961 and PhD degree from the Indian Institute of Science in 1967.

Summary

Twenty-five slender high strength concrete-filled steel tubular columns were tested in order to study the influence of eccentricity of force upon their strength and load-deflection response. The eccentricity was varied from that producing single curvature bending through to double curvature bending whilst the length of the column was kept constant. Predictions of column strength and force-deflection response were obtained using a deformation control method of analysis and conclusions are drawn on the basis of comparisons between measured and predicted data.

1. Introduction

Concrete-filled steel tubular (CFST) columns offer a number of advantages in both design and construction. The steel tube (i) acts as permanent formwork for the plastic concrete, (ii) provides well distributed reinforcement in the most efficient position to resist applied bending moments, (iii) confines the hardened concrete which increases its strain capacity and strength, and (iv) protects the surface of the concrete from physical damage and deleterious environmental effects such as carbonation. In turn, the concrete increases the critical buckling stress of the steel tube by changing its buckling mode. Overall, composite column construction enables (i) speed of construction to be improved, (ii) smaller cross-sectional dimensions for a given column strength, (iii) simple connections to steel floor beams which reduces the design time, and (iv) higher impact and seismic resistance.

Test data on the behaviour of CFST columns which incorporate low or medium strength concrete, together with guidelines for their design, are available in the literature, but very little is known about such columns when they are made of high-strength materials. This paper describes the results of 25 tests on high strength circular CFST columns (Kilpatrick and Rangan 1997) and compares these with the predictions of a deformation-control method of analysis.

2. Materials, Specimens and Equipment

All specimens were constructed using commercially available circular hollow steel tube which was manufactured by cold-forming and high frequency electric resistance welding. Tests showed

that the 101.5 mm × 2.4 mm ($D_o \times t$) tube had a 0.2% offset tensile strength of 410 MPa and an ultimate tensile strength of 475 MPa.

The 10 mm aggregate high-strength concrete was commercially supplied. Standard tests conducted on ten 100 mm diameter cylinders showed the average unconfined compressive strength to be 96 MPa. In addition, two 150 mm diameter cylinders were tested to determine the modulus of elasticity which was found to be an average of 40 500 MPa.

After facing both ends of the empty steel tube in a lathe, each column was secured in a vertical position and filled with concrete in layers which was in turn compacted by an immersion vibrator. The length of each column was kept constant at 2175 mm centre-to-centre of male knife edges.

Testing of the columns was carried out using a 2500 kN capacity Avery-Denison universal testing machine. Both ends of each column were clamped to specially made hardened knife-edge assemblages which had been previously located on the top and bottom platens of the testing machine. The eccentricity of the applied compressive force was obtained by displacing the end of the column laterally from the axis of the testing machine. During the test simultaneous recordings were made of the applied force and lateral deflections of the columns at mid-height and quarter-height. After the recording system was initialised, the testing machine ram was moved upwards at a steady rate of approximately 1 mm/min until it became apparent that the limit of either the knife-edge assemblages or the LVDT at mid-height was approached.

3. Results

A summary of the test programme and the measured column strengths is given in Table 1.

Col. no.	Force eccentricity top, btm (mm)	Measured strength (kN)	Col. no.	Force eccentricity top, btm (mm)	Measured strength (kN)	Col. no.	Force eccentricity top, btm (mm)	Measured strength (kN)
SC-16	+50,+50	157	SC-25	+40,+10	243	SC-34	+20,0	367
SC-17	+50,+30	183	SC-26	+40,0	260	SC-35	+20,-10	411
SC-18	+50,+20	196	SC-27	+40,-10	281	SC-36	+40,-30	344
SC-19	+50,+10	215	SC-28	+40,-20	331	SC-37	+40,-40	385
SC-20	+50,0	237	SC-29	+30,+20	244	SC-38	0,0	523
SC-21	+50,-10	256	SC-30	+30,0	318	SC-39	+50,-30	303
SC-22	+50,-20	266	SC-31	+30,-10	340	SC-40	+50,-50	344
SC-23	+50,-20	266	SC-32	+30,-20	384			
SC-24	+40,+30	197	SC-33	+20,+20	282			

Column SC-23 was a repeat of column SC-22.

Table 1 Slender column test programme

4. Method of Analysis

A simple iterative displacement-controlled method of analysis, fully described elsewhere (Kilpatrick 1994, 1996), was used to predict the complete short-term force-deformation response of the tested columns. The method requires prior knowledge of the moment-thrust-curvature

relationships of the cross-section of the column which can be obtained using the technique described by Warner et al (1989). For eccentrically loaded columns subjected to combined thrust and bending, the analytical procedure is as follows:

1. Discretise the column into n rigid segments of length ΔL with n+1 nodes.
2. Choose a value of the control slope θ_0 applied at node 1 at the bottom of the column
3. Select a trial value of the force N.
4. For the current value of N generate the corresponding moment-curvature relation up to the point at which the maximum moment capacity $M_{i\,max}$ is realised.
5. For all nodes along the column, calculate the deflection v_j of node j from the initial (unloaded) position of the column using Eq. (1), (2) and (3).

$$v_j = v_{j-1} + \Delta v_j + \Delta\theta_{j-1}\,\Delta L \quad (1)$$

$$\Delta\theta_{j-1} = \kappa_{j-1}\,\Delta L \quad (2)$$

$$\Delta v_j = v_{j-1} - v_{j-2} \quad (3)$$

In using Eq. (2) the curvature κ_{j-1} at the previous node j-1 is obtained from the moment-thrust-curvature relationship by satisfying the equilibrium requirement that the (internal) moment capacity of the cross-section must equal the (external) moment $M_{e\,j-1}$ given by

$$M_{e\,j-1} = N(e_{j-1} - v^{i}_{j-1} - v_{j-1}) \quad (4)$$

The moment-thrust-curvature relationship which must be used depends upon whether the bending moment at the node has increased or decreased compared with the previous successful solution. If the bending moment has increased then the moment-curvature relation generated previously in step 4 is used. However, if the bending moment has decreased then it is assumed that the section follows an unloading line whose slope is equal to that of the initial (zero load) tangent stiffness of the moment-force-curvature relationship of the previous successful solution for the node.

6. Check the misclose at node n+1 at the top of the column. If the magnitude of the force N is precisely correct then the displacement v_{n+1} will be zero, but rounding off and approximation errors will make this event unlikely. It is therefore usual to prescribe a tolerance to the error which is permissible and a value of ±0.5% of the largest deflection along the column was adopted in the present study. Data on the deflected shape and distributions of moments and curvatures may be printed. A new increased value of the control slope θ_0 is selected and the process returns to step 2. If v_{n+1} is not within the prescribed tolerance limit, a new value of N must be selected and the process returns to step 4. If, for the current value of the control slope, the process will not converge after a specified number of trials then it should be stopped because the solution lies on or very close to the section capacity line. Plots of the section capacity line and the force N versus its total eccentricity at the critical section may then be constructed.

5. Analysis of Test Data

A modified version of the stress-strain relationship for concrete confined by a steel tube proposed by Tomii (1991) was used for the concrete in compression: the tensile strength of the concrete was neglected. The curvilinear stress-strain relationship for the steel in both tension and compression was approximated by seven linear segments. Complete details of the material properties are provided elsewhere (Kilpatrick 1996, Kilpatrick and Rangan 1997). Each column

was discretised into segments whose length was approximately equal to $D_0/2$. To simulate the (stiffening) effect of the knife edge/clamp assemblages at each end of the column, the nodes in these portions were assumed to possess an infinitely stiff moment-curvature relationship. Predictions of the strength of the eccentrically loaded columns are given in Table 2.

Col. no.	Column strength (kN)		Measured/ Predicted	Col. no.	Column strength (kN)		Measured/ Predicted
	Measured	Predicted			Measured	Predicted	
SC-16	157	154	1.019	SC-29	244	247	0.988
SC-17	183	180	1.017	SC-30	318	312	1.019
SC-18	196	196	1.000	SC-31	340	354	0.961
SC-19	215	213	1.009	SC-32	384	406	0.946
SC-20	237	232	1.022	SC-33	282	280	1.001
SC-21	256	252	1.016	SC-34	367	371	0.989
SC-22	266	274	0.971	SC-35	411	436	0.943
SC-23	266	274	0.971	SC-36	344	366	0.940
SC-24	197	199	0.990	SC-37	385	437	0.881
SC-25	243	241	1.008	SC-38	523	-	-
SC-26	260	267	0.974	SC-39	303	298	1.017
SC-27	281	296	0.949	SC-40	344	369	0.932
SC-28	331	328	1.009		*Col. SC-38 concentrically loaded*		

Table 2 Predictions of column strength

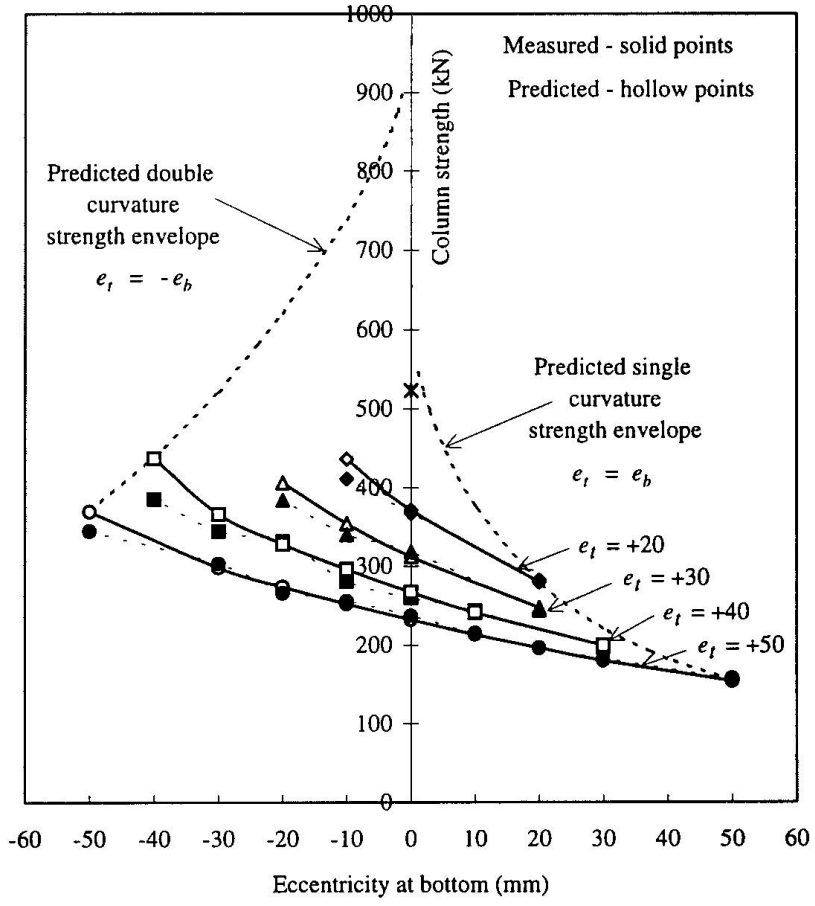

Figure 1 Measured and predicted column strengths

6. Discussion and Conclusions

6.1 Column strength

The mean value of the ratio of measured/predicted column strengths given in Table 2 of 0.982 and standard deviation of 0.036 indicate excellent correlation. Figure 1 presents an interesting pictorial comparison between measured and predicted column strengths. Predicted strengths are shown for contours of constant eccentricity at the top of the column, with values of eccentricity at the bottom varying between equal to the top eccentricity and equal and opposite to the top eccentricity. Measured and predicted strengths generally compare better for cases of single curvature bending than for double curvature bending. Also shown in Fig.1 are the predicted strength envelopes which join the limiting values of eccentricity. The envelope of equal eccentricity top and bottom shows a rapid increase in column strength towards an estimated 580 kN under axial compression. A similar trend is evident in the envelope of strength for equal and opposite eccentricity of force. Although the type of the curve is similar to that of the other envelope, the rate of increase is greater. Moreover, the envelope approaches a column strength under concentric loading of about 930 kN. This limit is appreciably higher than that of the single curvature envelope because of the reduced theoretical effective length.

6.2 Force-deflection responses

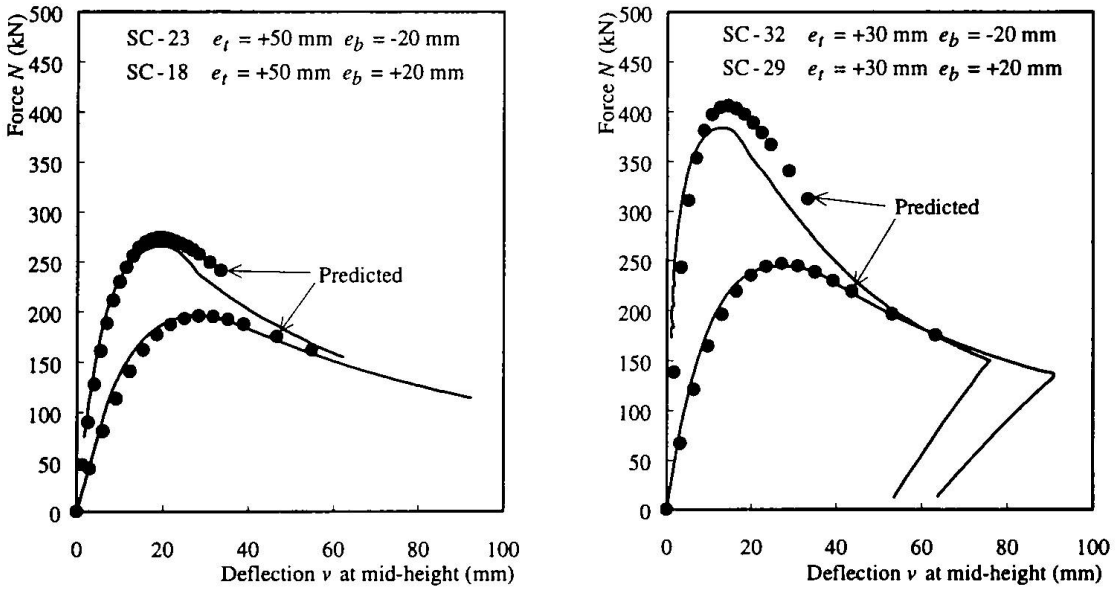

Figure 2 Measured and predicted force-deflection responses

Comparisons between measured and predicted responses for selected columns are given in Fig.2. Generally, the best correlations were obtained for the columns bent into single curvature, particularly those whose eccentricities were large.

6.3 Error analysis

The response of a column is influenced primarily by its length (slenderness) and the (primary) eccentricities of force at its ends. Given that it is a comparatively easy matter to accurately

determine the length of a column the most likely source of (significant) error in the tests is the magnitude(s) of the primary eccentricity of force. A study was undertaken (Kilpatrick 1996) of the sensitivity in the strength of the columns to variations in the magnitudes of these eccentricities. A realistic absolute error of 1 mm (1% of the column diameter) in each eccentricity was chosen for the purpose of the exercise. Thus, column SC-40 which had nominal eccentricities of +50 mm and -50 mm was reanalysed firstly for eccentricities of +51 mm and -51 mm, and secondly for +49 mm and -51 mm. Other columns were similarly analysed. As expected, it was found that the strength of the column under the second set of modified eccentricities was severely reduced because the columns could no longer exhibit a perfect anti-symmetrical deflected shape, and began to unwrap as loading advanced.

Col. no.	Eccentricity top, btm (mm)	Column strength (kN)	Eccentricity top, btm (mm)	Column strength (kN)	Eccentricity top,btm (mm)	Column strength (kN)
SC-40	+50,-50	369	+51,-51	363	+49,-51	347
SC-37	+40,-40	437	+41,-41	429	+39,-41	401
-	+30,-30	520	+31,-31	511	+29,-31	458
-	+20,-20	619	+21,-21	608	+19,-21	512
-	+10,-10	737	+11,-11	724	+9,-11	551

Table 3 Effect of errors in eccentricity upon predicted column strength

6.4 Conclusions

The excellent correlation between measured and predicted data suggests that the deformation control method of analysis can reliably predict both the strength and entire force-deflection relationship of eccentrically loaded circular CFST columns. Small variations in eccentricity have little effect upon the predicted response of a column bent into single curvature but a pronounced effect for columns bent into double curvature.

References

KILPATRICK A.E. (1994), 'Response of Composite Columns to Applied Axial Shortening', *Proceedings, Fourth International Conference on Steel-Concrete Composite Structures*, ASCCS, Kosice, Slovakia, June, pp. 218-221.

KILPATRICK A.E. (1996), 'The Behaviour of High-Strength Composite Concrete Columns', PhD thesis, Curtin University of Technology, Perth, Australia, September, 317 pp.

KILPATRICK A.E. and RANGAN B.V. (1997), 'Tests on High-Strength Composite Concrete Columns', Civil Eng. Research Report No. 1/97, Curtin University of Technology, Perth, Western Australia, March.

TOMII M. (1991), 'Ductile and Strong Columns Composed of Steel Tube, Infilled Concrete and Longitudinal Steel Bars', Special Volume, *Proceedings, Third International Conference on Steel-Concrete Composite Structures*, ASCCS, Fukuoka, Japan, Sept., pp. 39-66.

WARNER R.F., RANGAN B.V. and HALL A.S. (1989), 'Reinforced Concrete', Third Edition, Longman Cheshire, 553 pp.

Structural Behaviour of Concrete-Filled Steel Box Sections

Jun Yeup SONG
Post Graduate Student
Yeungnam University
Taegu, S/Korea

Jun Yeup Song, born 1968
received M.A. at Youngnam
University in S/Korea

Young Bong KWON
Assistant Professor
Yeungnam University
Taegu, S/Korea

Young Bong Kwon, born 1954
received M.A. at Seoul National
Univ. 1983 and Ph.D. at Univ.
of Sydney 1992

Summary

An experimental study on the behavior of concrete-filled steel box stub columns was performed. Steel box columns with and without stiffeners were also tested under concentric compressive load to failure. The result of the test showed composite box columns had high ductility as well as high strength due to mutual confinement between concrete and steel plate. In addition, simple formulas for design of composite column were proposed based on the test results.

1. Introduction

The concrete-filled steel box column has a lot of advantages such as high strength, high ductility and large energy absorption capacity, so that it has become increasingly popular in various kinds of structures. Especially, its excellent earthquake-resistant properties have proved recently in other countries, hence it is strongly needed to investigate the behavior of composite columns.

2. Test Specimen

2.1 Material Properties

The tensile coupon test was performed to determine the mechanical properties of the steel used(SS400 : nominal yield stress σ_y = 2400 kg/㎠). The results given in Table 1. show higher yield and ultimate strength than the nominal strength because of the welding and cutting from test specimens. To determine the compressive strength of the concrete, 15 cylinders (10cm diameter x 20cm height) were cast from the same concrete used inside the concrete-filled column. The cylinders were made with a water/cement ratio of 50% from ordinary portland cement and well graded aggregate(maximum size = 19mm) and were cured for 28 days until the column specimens were tested. The average values obtained 15 cylinders are listed in Table 1.

2.2 Shapes, Labeling and Size

Six concrete-filled steel box columns and seven steel box columns with and without longitudinal stiffeners were tested to compare the ultimate strength, ductility and postbuckling strength. In the case of the stiffened steel box column,

specimens were classified again as spot welding and fillet welding to determine the effect of welding. In Table 2, the numerals following the letter US, UC, SS are related to the value of equivalent width-thickness ratio parameter R. Buckling coefficient k in the case of the SS series was decided by the numerical analysis using Bfplate(Lau and Hancock 1986)[1] as 5.45 because the number of subpanels in the web and flange are different.

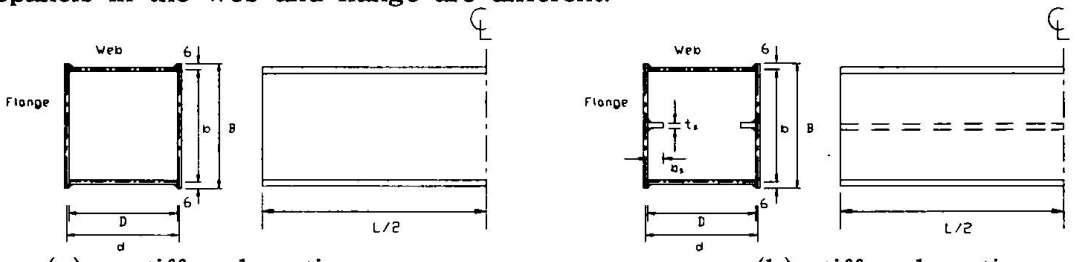

(a) unstiffened section (b) stiffened section

Fig. 1 Test specimens

Table 1. Material properties

Steel	E_s (kg/cm²)	ν	σ_y (kg/cm²)	ε_y	σ_u (kg/cm²)	ε_u
	2,057,000	0.3	3,200	0.001560	4,940	0.002401

Concrete	Days	E_c (kg/cm²)	f_c (kg/cm²)	*β x f_c (kg/cm²)	*β = 0.7 [2]
	28	288000	307	259	

Table 2. Measured dimensions of test specimens

Unstiffened Steel box column	Specimen	b (cm)	t (cm)	A_s (cm²)	L (cm)	b/t	R (k=4.0)
	US 9	13.0	0.32	17.3	39.0	40.6	0.84
	US 12	17.5	0.32	22.3	52.5	54.7	1.14
	US 15	22.0	0.3	26.94	66.0	73.3	1.43
Unstiffened Concrete-filled box column	Specimen	b (cm)	t (cm)	A_c (cm²)	L (cm)	b/t	R (k=4.0)
	UC 9	13.0	0.32	168	39.0	40.6	0.84
	UC 12	17.5	0.32	306	52.5	54.7	1.14
	UC 15	22.0	0.3	483	66.0	73.3	1.43

Stiffened Steel box column	Specimen	b(cm)	b_s(cm)	L(cm)	t(cm)	t_s(cm)	A_s(cm²)	R(k=5.45)
	SS15 (2.5)	22	2.5	66	0.3	0.3	28.61	1.3
	SS15 (3.5)	22	3.5	66	0.3	0.3	29.2	1.3
	SS15 (4.5)P	22	4.5	66	0.3	0.3	29.8	1.3
	SS15 (4.5)F	22	4.5	66	0.3	0.3	29.8	1.3

2.3 Residual Stress

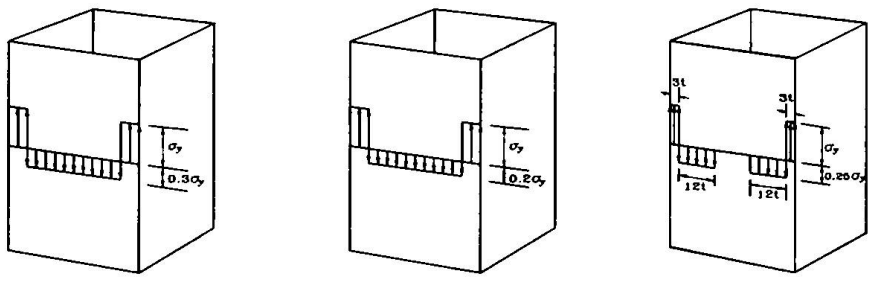

(a) RS 1 [2] (b) RS 2 [3] (c) RS 3

Fig. 2 Assumptions of residual stresses distribution

In this investigation, three types of residual stress were assumed as Fig.2 to

conduct the inelastic buckling analyses and compare with the results of the test.

3. Test Results

3.1 Test Arrangements

The axial displacement was measured using four displacement transducers equipped at each edge of loading plate and the strain was measured with eight strain gages attached at the center of plates. To assure uniform compression and prevent the eccentricity, very thick loading plates(t=4cm) were attached at each end(top and bottom) of test specimens and preliminary tests were carried out within the elastic range by adjusting the loading plate, based on the measurements of strain and displacement. The loading process was paused at every step of 5 tons for a minute to determine the difference between static and dynamic load.

3.2 Failure Modes

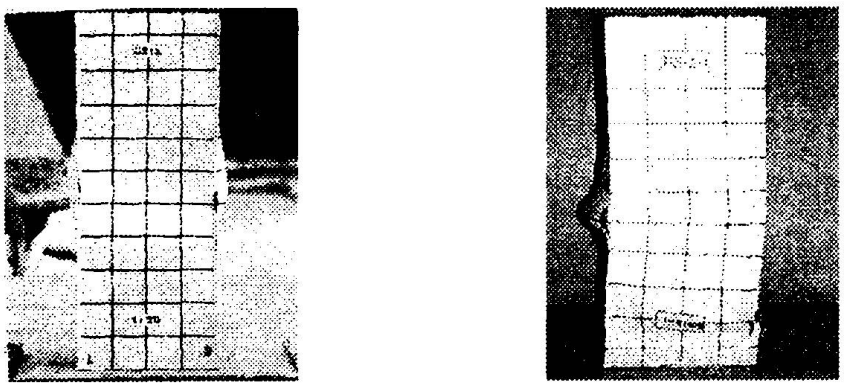

(a) steel column (US12) (b) concrete-filled steel column (UC12)

Fig. 3 Buckling modes of test specimens

In the case of the steel box columns, it was observed that local buckling failure of the plate panels occurred before the maximum load was reached and local buckling shaped three half-waves along overall length of the specimens due to aspect ratio a/b=3.0 as shown in Fig. 3(a). A very symmetric buckling mode, at the two opposite faces of the specimens buckled inward and at the other two perpendicular faces buckled outward, against the axes of the cross section was observed at the central part of the specimens.

In the case of the 9 series concrete-filled columns, it was observed that local plate buckling occurred in one of the plates of the column just before maximum load was reached. As an increment of width-thickness ratio, the occurrence of local buckling came earlier and that could be seen at steel box columns. Since the failure of concrete-filled columns was controlled by the fracture of concrete, buckling of plates in concrete-filled columns showed asymmetric buckling mode against the axes of the cross section as shown in Fig. 3(b). All steel panels buckled outward because the buckling of the steel plate toward inside was prevented by the filled-in concrete. After the local buckling of the plates, deformation rapidly increased and cracks occurred in the weld.

3.3 Results and Design Curves

Table 3. shows the comparison between test results and inelastic buckling analysis using B_3-Spline Finite Strip Method(Bfplate). In this comparison, test result of US9 indicates in good agreement with RS1 and in the case of US12, US15, good agree with RS3. It was supposed that US9 was much effected by welding because width b is relatively small.

Table 3. Test results of unstiffened steel box columns

Specimen	P_u (ton)	σ_u (kg/cm^2)	σ_b (kg/cm^2)				σ_u/σ_y		σ_b/σ_y	
			Test	Inelastic analysis			Test	Prediction (Eq. 2.6)	Test	Inelastic analysis
				RS 1	RS 2	RS 3				
US 9	52.25	3034	2601	2692	2945	3198	0.94	0.90	0.81	0.84
US 12	60.40	2709	2317	1781	2014	2398	0.84	0.73	0.72	0.75
US 15	54.68	2030	1305	668	911	1326	0.63	0.62	0.41	0.41

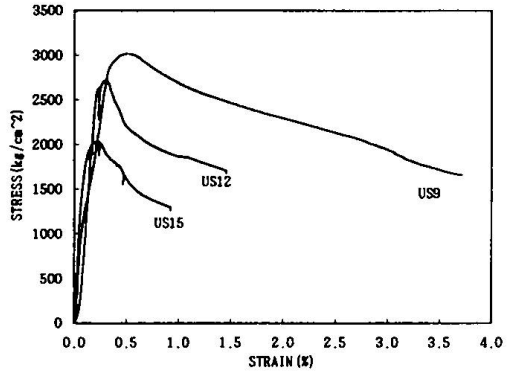

Fig. 4 Stress-strain curves (unstiffened steel column)

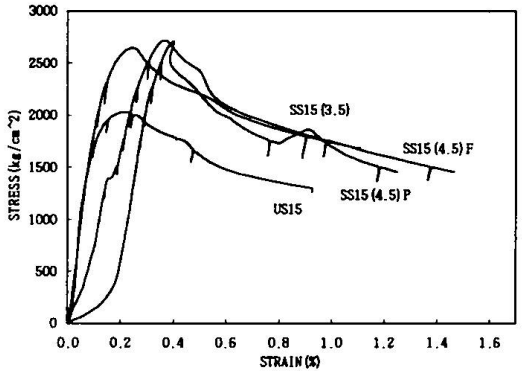

Fig. 5 Stress-strain curves (stiffened steel column : SS15)

Stress-strain curves of unstiffened steel columns were shown in Fig.4. It is noted that the ultimate and buckling stress of steel box columns were reduced as the width-thickness ratio of the section is increased. In Fig. 5, the stress-strain relation of SS15(4.5)P (spot welding) after ultimate load shows unstable behavior, that was supposed to be caused by separation of the stiffeners and plates as deformation getting serious after peak load. The ultimate strengths of SS15(4.5)P and SS15(4.5)F (fillet welding) were nearly same and somewhat higher than SS15(3.5). The comparison between US15 and SS15 shows that ultimate load of stiffened steel column higher than unstiffened steel column's about 40~50% and about 30~40% in the buckling stress. This means that longitudinal stiffeners which have enough stiffness to resist the distortional buckling of the section can be very effectively used as a column member due to the increase of buckling and postbuckling strength reserve.

Table 4. Test results of stiffened steel box columns

Specimen	P_u (ton)	σ_u (kg/cm^2)	σ_b(kg/cm^2)				σ_u/σ_y		σ_b/σ_y	
			Test	Inelastic analysis			Test	Prediction (Eq. 2.7)	Test	Inelastic analysis
				RS 1	RS 2	RS 3				
SS15 (3.5)	77	2637	1660	1241	1509	1627	0.82	0.73	0.52	0.51
SS15(4.5)P	81	2718	1720	-	-	-	0.85	0.72	0.54	-
SS15(4.5)F	81	2718	1715	1242	1510	1629	0.85	0.72	0.54	0.51

A similar design formula to that used by Chajes et al.(1966)[4] for inelastic flexural-torsional buckling stress was adopted for determining the inelastic local

buckling stress of the tubular columns. The proposed formula(called design proposal 1) is given by

$$\sigma_b = \sigma_{be} \qquad (\sigma_{be} \le 0.5\sigma_y)$$

$$\sigma_b = \sigma_y\left(1 - \frac{\sigma_y}{4\sigma_{be}}\right) \qquad (\sigma_{be} > 0.5\sigma_y)$$

---------- (Eq. 1)

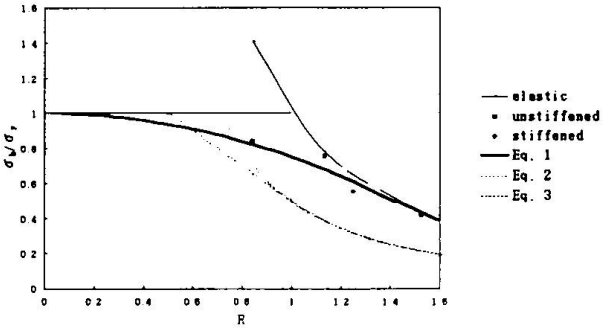

Fig. 6 Comparison of test results with design proposal 1

A comparison of design proposal 1(Eq. 1) with $\frac{\sigma_b}{\sigma_y} = \frac{0.5}{R^2}$ for unstiffened plate (Eq. 2) and $\frac{\sigma_b}{\sigma_y} = 1.5 - R$ $(0.5 < R \le 1.0)$ or $\frac{\sigma_b}{\sigma_y} = \frac{0.5}{R^2}$ $(1.0 < R)$ for stiffened plate (Eq. 3) in Korean Standard Specifications for Highway Bridges[5] and test results is shown in Fig. 6.

In the case of steel box column, an alternative design approach(called design proposal 2) using ultimate stress is also proposed as $\frac{\sigma_u}{\sigma_y} = \frac{0.8}{R^{0.7}}$ $(R > 0.73)$ for unstiffened plate(Eq. 4) or $\frac{\sigma_u}{\sigma_y} = \frac{0.8}{R^{0.4}}$ $(R > 0.57)$ for stiffened plate(Eq. 5), in this paper. It is based on the idea that Eqs. have no regard of postbuckling strength reserve. The second proposal and test results are plotted in Fig. 7.

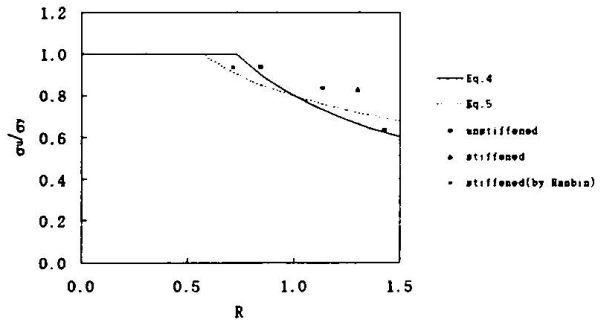

Fig. 7 Comparison of test results with design proposal 2

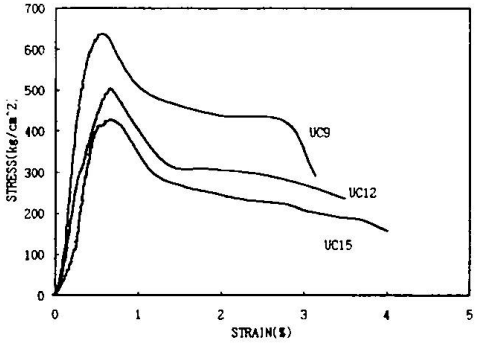

Fig. 8 Stress-Strain Curve (Concrete-Filled Columns)

The behavior of the UC series column is different from those of hollow steel tubular columns because of filled-in concrete. Sudden local buckling occurred after peak load due to brittle fracture of concrete at UC series. The concrete-

Table 5. Test results of unstiffened concrete-filled columns

Specimen	P_u (ton)	P_b (ton)	$P_y = \sigma_y A_s + \beta f_c A_c$ (ton)	σ_b/σ_y
US 9	118.5	98	98.9	0.99
US 12	166	140	150.6	0.93
US 15	246	160	211.3	0.76

filled section shows good structural performance such as higher strength and ductility than the hollow steel column, since steel and concrete confined each other. Eq. 6 proposed by Nakai et al.[6] and the test results of concrete-filled columns were plotted in Fig. 9.

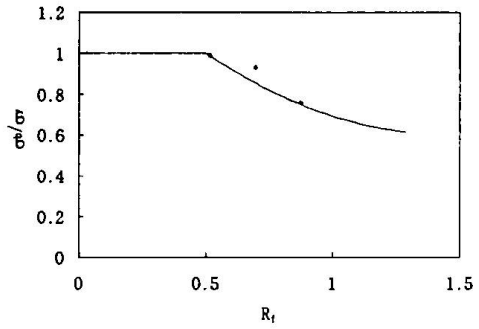

$$\frac{\sigma_b}{\sigma_y} = 0.433\,(R_f - 0.5)^2 - 0.831\,(R_f - 0.5) + 1.0 \quad (0.5 < R_f < 1.3) \qquad \text{(Eq. 6)}$$

R_f : substitution for k=10.67 in R (plate with fixed loading-fixed unloading edges)

Fig. 9 Comparison of test results with Eq. 6

4. CONCLUSIONS

A series of compression tests on steel columns with and without stiffeners and concrete-filled columns has been performed. In the case of the column with the stiffener, spot welding has lots of advantages in construction with convenience and decrease of residual stress. The use of the longitutional stiffener with adequate stiffness is more economic manners than the way to increase the thickness of the panel. Concrete-filled column showed much higher ductility as well as strength than hollow steel columns. As increment of width-thickness ratio parameter R, although local buckling occurred, the concrete-filled columns showed considerable postbuckling strength reserve before fracture.

APPENDIX I. Reference

[1] Lau, S.C.W. and Hancook, G.J. "Buckling of Thin Flat-Walled Structures by a Spline Finite Strip Method", Thin-Walled Structures, Vol.4, No.4, pp.269-294, 1986
[2] Ge, Hanbin, and Usami, T. "Development of Earthquake-Resistant Ultimate Strength Design Method for Concrete-Filled Steel Structures", Nagoya University, March, 1994
[3] Kim, W.S., Kwon, W.B., "A study on the Residual stresses in Rolled and Built-up Sections", The conference Report of Korean society of steel construction, pp.95-103, 1994
[4] Chajes, A., Fang, P.J. and Winter, G., "Torsional-Flexural Buckling, Elastic and Inelastic, of Cold Formed Thin-Walled Columns", Research Bulletin, No.66-1, School of Civil Engineering, Cornell University, Ithaca, New York, 1966
[5] "Korean Standard Specifications for Highway Bridges", 1996
[6] Nakai, H., Kitada, T., and Yoshikawa, O. "A Design Method of Steel Plate Element in Concrete-Filled Square Steel Tubular Columns" Proc. of JSCE, I-3, pp.405-413, 1985

APPENDIX II. Notation

E_s, E_c = Young's modulus of steel and concrete, respectively;
σ_y = yield stress; σ_u = ultimate stress; ϵ_y = yield strain of steel;
f_c = compressive strength of concrete; ν = Poisson's ratio of steel;
L = column length; b = plate width; t = plate thickness;
A_s, A_c = crosssectional area of steel and concrete, respectively;
R, R_f = plate width-thickness ratio parameters; $R = \sqrt{\frac{\sigma_y}{\sigma_{cr}}} = \frac{b}{t}\sqrt{\frac{12(1-\nu^2)}{\pi^2 k}}\sqrt{\frac{\sigma_y}{E}}$
k = buckling coefficient($4n^2$); n = number of subpanels in each plate panel;
σ_b = inelastic buckling stress; σ_{be} = elastic buckling stress;

Ductility and Strength of Thin-Walled Concrete Filled Box Columns

Brian UY
Lecturer in Civil Engineering
University of Wollongong
Wollongong, NSW, Australia

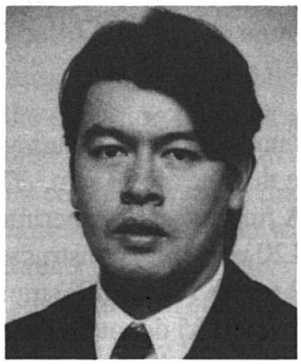

Brian Uy, born in 1970 received his Bachelors and Doctorate in Civil Engineering from the University of NSW. Since graduation he has worked on the design of multistorey buildings with Ove Arup and Partners, Sydney and he is currently lecturing in structural engineering. His main research interests include the application of composite construction in multistorey buildings.

Summary

This paper is concerned with the ultimate strength and ductility of thin-walled concrete filled steel box columns. An extensive set of experiments on concrete filled thin-walled steel box columns will be presented and comparisons with a numerical model will be made. Included in this paper are experimental results and comparisons of box columns filled with normal strength and high strength concrete. Ultimate strength and ductility obtained from test results is used to calibrate the numerical model and to monitor the effects of the use of the increased concrete strengths.

1. Introduction

Concrete filled steel box columns have undergone a renaissance in Australian tall building construction over the last decade due to the increased economies established by reduced construction times and structural costs (Watson and O'Brien[1], Bridge and Webb[2]). The use of very thin walled steel boxes reduces the capital outlay of steel which is a relatively expensive construction material. The concrete pumping operation which takes place after many levels of construction have been completed then speeds the rate of construction which further reduces the overall structural cost. The development of high strength concrete has made the use of concrete filled steel columns extremely attractive as the relatively inexpensive concrete is utilised to resist compressive forces more efficiently than the steel plate. The increased use of high strength concrete needs to include a study of the effects of the concrete strength on the ductility and strength of the structural member. This is particularly important in the design of frames for lateral loading which are designed to fail with strong columns and weak beams. This failure mode needs to be assisted with sufficient rotation capacity from the structural member and it is therefore necessary to consider the ductility in relation to strength for concrete filled steel box columns.

This paper presents an experimental and theoretical study of the ductility and strength of concrete filled steel columns using very thin steel plate. A set of experiments is presented, using normal and high strength concrete and a numerical model developed elsewhere is used to compare the moment curvature response of the model to the experiments for varying thrusts. A method for the comparison of the strength interaction diagram for bending and compression is also presented for the theoretical and experimental results. With further development and experimental data this model can be used to develop design rules and relationships for structural engineers using these members in the design of buildings.

2. Experimental Programme

The aim of the experiments was to determine the cross-sectional strength of concrete filled thin-walled steel box columns subjected to combined axial compression and bending moment. This was achieved by testing stubby column specimens in combined compression and bending and testing beam specimens in pure bending. Furthermore the experiments were undertaken to compare the strength and ductility behaviour of concrete filled steel columns using normal and high strength concrete.

The normal strength concrete study was undertaken on columns which had an overall cross-section size of 180 mm with a steel plate thickness of 3 mm. The properties and characteristics of the specimens are outlined in Table 1. A further set of experiments which utilised high strength concrete having a cross-section size of 120 mm were constructed and tested. Full details of each of these specimens are shown in Table 2 where (C) and (B) represents the column and beam specimens respectively. Specimens NS5 and HS5 denoted as (LB) were tested by loading the steel only to determine the local buckling capacity and this is further dealt with by Uy[3]. The columns were tested under varying eccentricity until the failure load N_u was reached. The ultimate moment was calculated as $M_u=N_u.e$ for the columns and $M_u=N_uL/2$ for the beam specimens tested under two point loading. Figure 1 shows the normal strength concrete filled series after failure.

Specimen No.	b (mm)	t (mm)	f_y (MPa)	f_c (MPa)	e (mm)	N_u (kN)	M_u (kNm)
NS1 (C)	186	3	300	32	0	1555	0
NS2 (C)	186	3	300	32	37	1069	39.6
NS3 (C)	186	3	300	32	56	1133	63.4
NS4 (C)	186	3	300	32	84	895	75.2
NS5 (LB)	186	3	300	32	0	517	0
NS6 (B)	186	3	300	32	L=950	131	62.6

Table 1. Series 1 - Normal Strength Concrete Filled Box Columns

Specimen. No.	b (mm)	t (mm)	f_y (MPa)	f_c (MPa)	e (mm)	N_u (kN)	M_u (kNm)
HS1 (C)	126	3	300	50	0	1114	0
HS2 (C)	126	3	300	50	20	996	19.9
HS3 (C)	126	3	300	50	40	739	29.6
HS4 (C)	126	3	300	50	50	619	31.0
HS5 (LB)	126	3	300	50	0	454	0
HS6 (B)	126	3	300	50	L=600	93	27.9

Table 2. Series 2 - High Strength Concrete Filled Box Columns

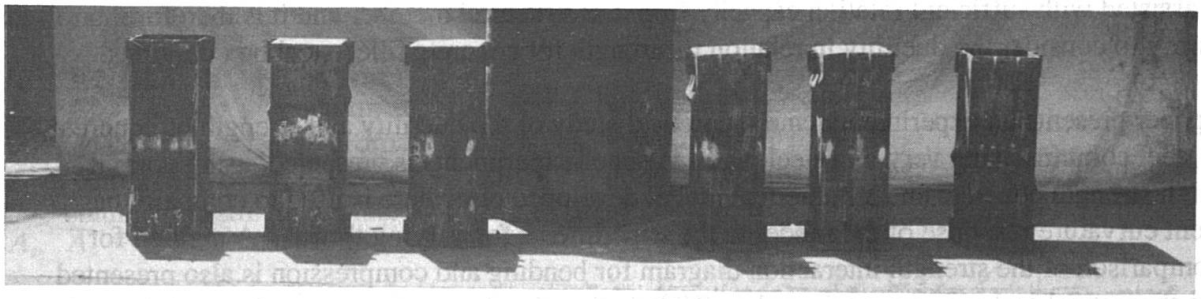

Fig. 1 Normal Strength Concrete Test Specimens after Failure

3. Numerical Model

A numerical model for the thrust moment-curvature behaviour developed by Uy[4] has been used to predict the behaviour of these columns. Pertinent points of this model are briefly described here.

3.1 Cross-Sectional Analysis Technique

A typical strain distribution over the cross-section is established in Fig. 2, and it is characterised by the strain ε_{top} at the top fibre and the curvature ρ. For a given curvature ρ, a position d_n for the concrete neutral axis depth was assumed, so that a strain distribution was obtained. The curvature ρ is the same in the steel and concrete core, so that if there is another neutral axis in the steel caused through slip, then it is uniquely defined. Slip was ignored in this analysis as the slip and slip strain measured in the experiments was negligible. The axial force N in the section was determined from a summation of the forces in each slice. The stress in each slice was expressed as a function of strain at the centroid of each slice, obtained using the relative material constitutive relationship. The concrete neutral axis depth d_n was incremented successively from d_n=0 by steps of D/20 until the value of N changed sign for pure bending or until the value of applied axial force was reached unity for the case of bending and compression. The method of bisections was then used to converge on the value of d_n for greater accuracy. The moments of the forces in each slice were then summed to produce the section moment M.

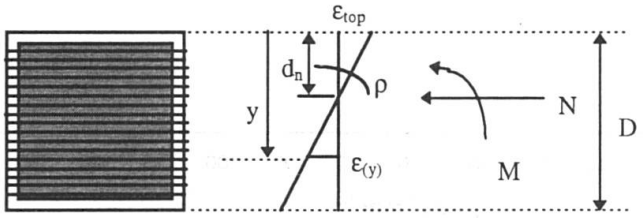

Fig. 2 Concrete Filled Box Section Typical Strain Distribution

This procedure was followed for increasing steps of curvature and steps of thrust to obtain the thrust moment curvature response, and so to observe either ductile or brittle behaviour. The steel was modelled as mild structural steel which is initially elastic linear then goes through a plastic range until strain hardening occurs upon which the steel increases in stress. The CEB-FIP model for the stress-strain relationship of concrete was utilised for the ensuing analyses, (CEB-FIP[5]). It should be noted that this stress-strain relationship is for unconfined concrete. For a steel box column local buckling may occur prior to the concrete crushing and thus the confinement effect can not occur and is thus conservatively ignored in the analysis.

3.2 Moment-Curvature Results

Using the method developed a moment curvature analysis was carried out on the cross-sections of the experiments for varying thrust. It was decided to use a thrust of 0, 25, 50 and 75 % of the maximum axial thrust N_u. The results of the analysis are shown in Figs 3 and 4 for normal and high strength concrete respectively where it is illustrated that the presence of axial force initially causes an increase in moment carrying capacity. However for higher levels of axial force the primary compression failure means that a reduced bending moment carrying capacity is caused. A reduction in the ultimate curvature is experienced for an increasing value of thrust.

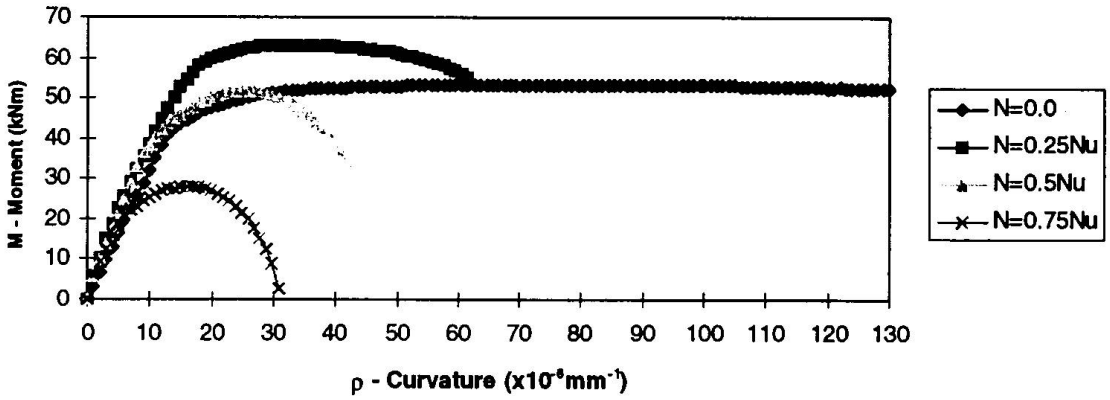

Fig. 3 Thrust-Moment-Curvature Response for Normal Strength Concrete Filled Columns

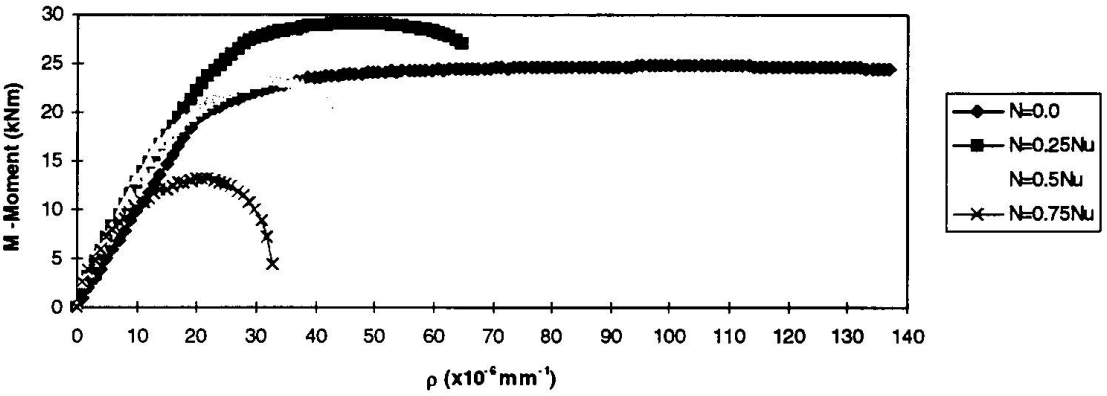

Fig. 4 Thrust-Moment-Curvature Response for High Strength Concrete Filled Columns

4. Comparisons

4.1 Ultimate Strength

The peaks of the moment curvature plots for varying thrusts are used to construct the strength interaction diagrams between axial force and bending moment. From Figs 3 and 4 the peaks of each curve are used to construct the strength interaction diagrams shown in Figs 5 and 6 for normal and high strength concrete respectively. The strength interaction diagrams are compared with the experimental results of Tables 1 and 2 in Figs 5 and 6. Firstly it should be noted that there is extremely good agreement for the case of pure axial force in both the normal and high strength concrete column cross-sections. Furthermore it is shown that the numerical model is conservative in it's estimate of the cross-sectional strength for both the normal and high strength concrete specimens. Thus the model presented should therefore be appropriate for design with the use of appropriate capacity reduction factors.

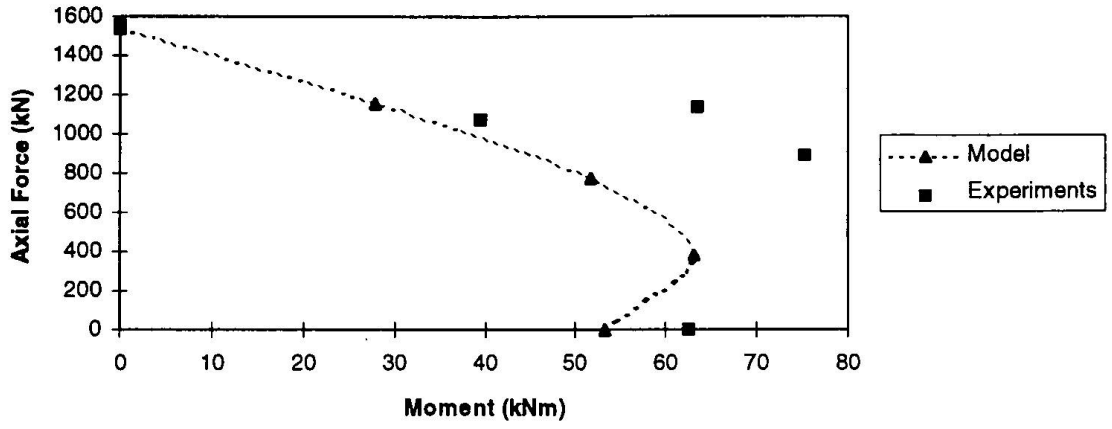

Fig. 5 Strength Interaction Diagram for Normal Strength Concrete Filled Columns

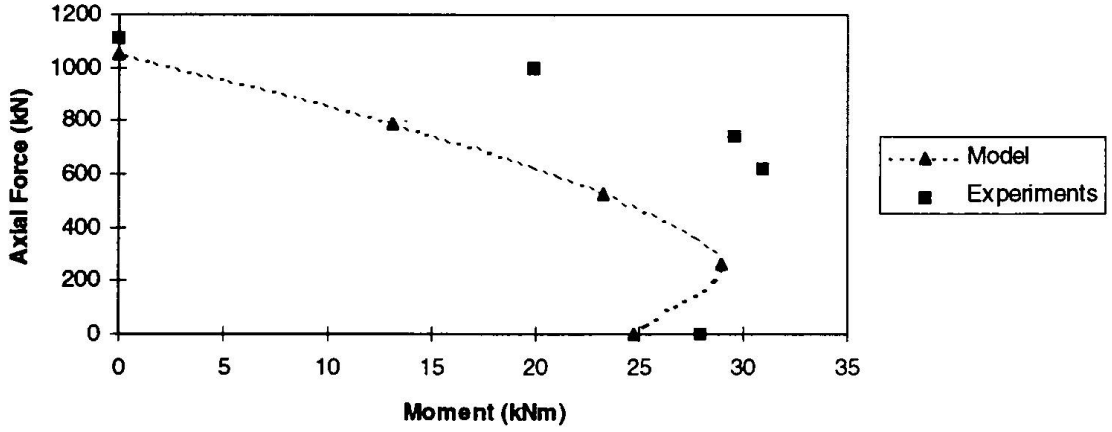

Fig. 6 Strength Interaction Diagram for High Strength Concrete Filled Columns

4.2 Ductility

The ductility ratio is calculated as the ratio of the ultimate curvature ρ_u to the yield curvature ρ_y where $\delta = \frac{\rho_u}{\rho_y}$. These ratios are calculated and compared for each of the specimens in Tables 3 and 4 for the experiments and theoretical model.

$\frac{N}{N_u}$	$\left(\frac{M}{M_u}\right)_{test}$	$\left(\frac{M}{M_u}\right)_{theory}$	$\delta_{theory} = \left(\frac{\rho_u}{\rho_y}\right)_{theory}$
0.0	1.0	1.0	9.56
0.25	1.20	1.18	4.42
0.5	1.01	0.97	2.80
0.75	0.63	0.52	1.62

Table 3. Normal Strength Ductility Ratios

$\frac{N}{N_u}$	$\left(\frac{M}{M_u}\right)_{test}$	$\left(\frac{M}{M_u}\right)_{theory}$	$\delta_{theory} = \left(\frac{\rho_u}{\rho_y}\right)_{theory}$
0.0	1.0	1.0	6.75
0.25	1.11	1.17	3.25
0.5	1.06	0.94	2.25
0.75	0.71	0.53	1.50

Table 4. High Strength Ductility Ratios

It is shown that the use of a higher strength concrete significantly reduces the ductility of a concrete filled steel column subjected to pure bending. However as the ratio of axial force is increased the apparent loss of ductility is less pronounced. As most columns under gravity load will have at least 40-50 % of the ultimate load as service loads it is therefore not as significant.

6. Conclusions

This paper has discussed the behaviour of concrete filled steel columns using both normal and high strength concrete. Experiments have been conducted to determine the cross-sectional strength and ductility of these two forms of columns. A numerical model developed elsewhere has been calibrated with these results with good agreement and has been found to be conservative in it's prediction thus rendering it appropriate for design. It is necessary to undertake more tests to adequately calibrate results which can therefore suggest design procedures particularly in relation to capacity reduction factors required for limits states or load resistance factor design.

7. Acknowledgements

The author would like to thank Messrs I.Bridge, S. Das, I. Laird, M. Lyon, I. Pratsas and R. Webb of the Department of Civil and Mining Engineering for fabrication, construction and conducting of the experiments outlined in this paper. The financial support of the Australian Research Council is acknowledged. Furthermore the author would like to thank BHP Slab and Plate Products Division, Port Kembla for the supply of the steel plate used for the columns.

8. References

1. Watson KB and O'Brien LJ. Tubular composite columns and their development in Australia. The Institution of Engineers Australia, Struct.Eng.Conf. Adelaide, 1990, pp. 186-90.
2. Bridge, R.Q. and Webb, J. Thin walled circular concrete filled steel tubular columns, Comp.Constr.in Steel and Concrete II, Proc.of an Engg Found.Conf. 1992, pp. 634-649
3. Uy, B. Slenderness limits for thin-walled steel concrete filled box columns, Composite Construction-Conventional and Innovative, 1997, pp.
4. Uy, B. Strength and ductility of fabricated steel-concrete filled box columns. *To appear in the* Proc.of the Engg Found Conf,: Comp. Constr. III, 1996, (In press).
5. Comite Euro-International du Beton-Federation Internationale de la Precontrainte, CEB-FIP Model Code for Concrete Structures, Paris, 1978, 348 pp.

Ductility of Steel Tube-Reinforced Concrete Composite Beams

Koji MAEGAWA
Prof. Dr-Eng.
Kanazawa University
Kanazawa, 920, JAPAN

Koji Maegawa, born 1952, received his doctoral degree of engineering in 1986 from the Graduate School of Nagoya University, Japan. His major study is the lateral-torsional instability of beams.
E-mail: maegawa@t.kanazawa-u.ac.jp

Summary

In this research, to improve the ductility of RC beams, the concrete-filled steel tubes (CFST) were employed instead of the round bars (RB) on the compression side. Two types of beams, i.e., the CFST-type beams and the RB-type beams were designed to have equal bending strength. A series of experiments was divided into two groups according to the loading patterns of static load and impact load. The experimental results show that the CFST improves the ductility capacity of beams more than two times in both cases of the loading patterns as compared with the RB.

1. Introduction

A great number of rock-sheds are constructed with the reinforced concrete (RC) or the pre-stressed concrete members and are widely used in Japan to protect vehicles against the falling rocks. The RC-beams used in the rock sheds are required to have the ductility capacity and the energy absorption capacity, because the design of such structures should be based on the energy absorption concept. The compression rupture of concrete governs the ductility capacity in the stage of small beam-deformation. Namely, the bending strength of RC beams decreases at the same time the compression reinforcing bars buckle after the rupture of concrete. Though the stirrups are arranged closely to improve the ductility capacity of RC beams, many stirrups are required to prevent the re-bars from buckling and to produce the confinement effect on the concrete in the compressive zone [1].

In this research, the concrete filled steel tubes (CFST) are employed instead of the round bars (RB) on the compression side to improve the ductility capacity of RC beams used in the rock sheds. Hereafter, such a RC beam and the RC beam with round bars on the compression side are referred as CFST-type beam and RB-type beam, respectively. The CFST-type beams are expected to have a high ductility capacity, because the CFST has a highest buckling load capacity. The CFST can also produce the confinement effect on the concrete filled into a steel tube [2,3].

A series of experiments was carried out on the CFST-type and RB-type beams subjected to two types of loading patterns, i.e., static load and impact load. The ultimate bending strengths of these specimens were designed to be equal. In this paper the ductility performance of such beams is discussed and evaluated from the experimental results. It is then remarked that the CFST improves the ductility capacity of beams more than two times as compared with the reinforcing bars usually used for the RC-beams.

2. Outline of Experiments

2.1 Test Specimens and Material Properties

Table 1 summarizes the tested specimens and material properties. Figure 1 shows the detailed dimensions of test specimens. All specimens are equally reinforced by three deformed bars on the tension side, but there is a difference in the compression reinforcements between CFST-beams and RB-beams. The stirrups are also arranged to prevent the shear force from affecting the beam strength.

(a)	Type of Specimen	CFST-beams					RB-beams			
	Compressive Reinforcement	2-Steel Tubes (ϕ60.5x2.3)					4-Round Bars (ϕ16)			
	Tensile Reinforcement	3-Deformed Reinforcing Bars (ϕ25)								
	Name of Specimen	C1	C2	C3	C4	CN	D1	D2	D3	D4
	Age at Loading (days)	38	40	114	111	39	38	40	114	111
	Concrete Strength (MPa)	52.5	54.2	54.4	51.4	52.8	52.5	54.2	54.4	51.4
	Test Program (Loading Type)	Static		Impact		Static			Impact	

(b)	Reinforcement Material	Steel Tube (ϕ60.5x2.3)	Round Bar (ϕ16)	Deformed Bar (ϕ25)
	Nominal Yield Point (MPa)	235	235	295
	Yield Point in tensile test (MPa)	406	369	408
	Ultimate Strength in test (MPa)	509	484	613

Table 1 (a) test specimens, (b) material properties

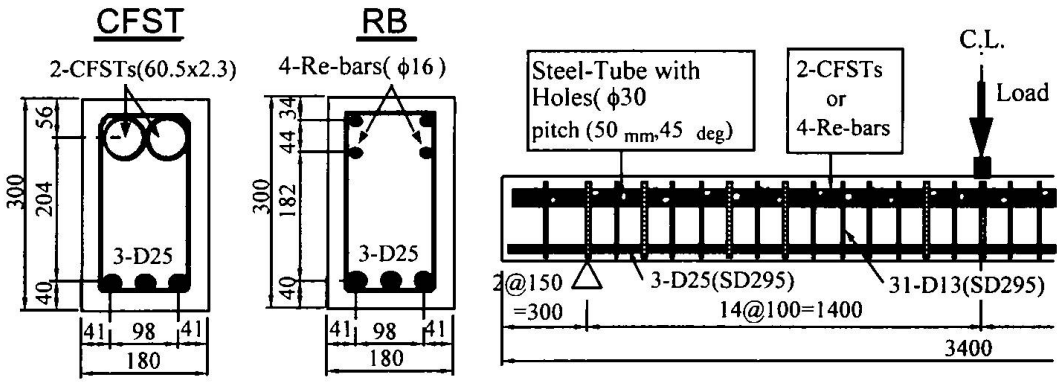

Fig. 1 Details of test specimens

Each specimen of CFST-beams has the same reinforcements of two mild-steel tubes on the compression side. In the specimens of C1, C2, C3 and C4, circular holes of ϕ30 *mm* are made along the tube-length at a distance of 50 *mm*, and are staggered with 45 *degrees* in the circumferential direction as shown in Fig. 1. These holes can form a series of concrete dowels which act in shear to resist the shear flow. Through these holes it is also easy to fill up the steel tube with concrete. The steel tubes without hole are used in the specimen CN for a comparison sake.

Each specimen of RB-beams D1, D2, D3 and D4 has the same reinforcements of four round bars on the compression side. Namely, RB-beams are the so-called doubly reinforcements-beams. The whole centroid-location and the total cross-section area of the four bars are almost equal to those of the steel tubes of CFST-beams. Therefore there is little difference in the nominal ultimate bending strengths between CFST-beams and RB-beams when the holes of steel tubes are not considered in CFST-beams. Using the section partitioning method, the design strength of concrete of 30 *MPa* and the nominal yield stress of reinforcements, the ultimate bending strengths of 96.0 *kNm* and 96.3 *kNm* are obtained for CFST-beams and RB-beams, respectively.

2.2 Test Procedures

The test program is divided into two groups according to load types. The first group of C1, C2, CN, D1 and D2 beams and the second group of C3, C4, D3 and D4 beams were tested under the static load and an impact load, respectively. In all experiments, the specimen is simply supported with the span length of 2.8 *m*, as shown in Fig. 1. A central point load is applied to the specimen through a steel rectangular block having the contact surface of 5 *cm* x 18 *cm*.

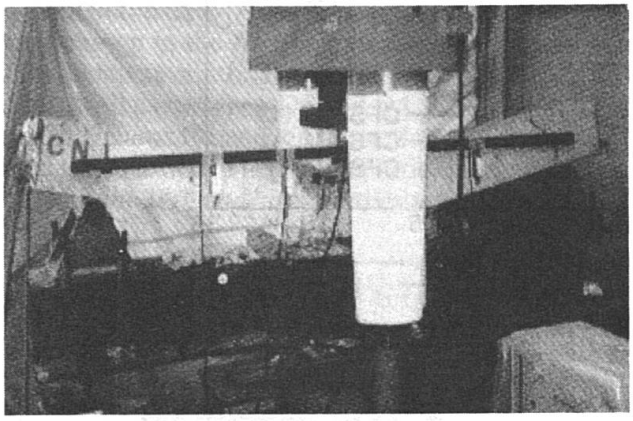

Fig. 2a Test set-up in statically loading

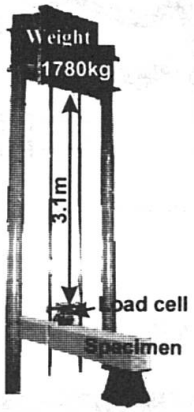

Fig. 2b Impact loading

2.2.1. Static Loading
In the static loading tests, a conventional compression testing machine shown in Fig. 2a was used and the ram stroke at a speed of 0.5 *mm/min* was applied in the early stage of loading. After the yield load of the tension reinforcement the test was continued at a ram speed of 4 *mm/min*. Loads, beam deflections and reinforcement strains were measured.

2.2.2. Impact Loading
In the impact loading tests, an assembled iron block of 1780 *kg* weight is set free falling from 3.1 *m* height to the specimen as shown in Fig. 2b. There is no rig preventing the beam from bounding. A load-cell, on which the free-fall weight hits directly, is set on the specimen. Instead of measuring the beam displacement at the loading point, the weight movement is measured by means of a displacement transducer connected to the weight by a wire. Data of strain-gauges, a load cell and the displacement and deceleration transducers were recorded in 0.2 msec sampling intervals.

3. Test Results and Considerations

3.1 Statically Loading Tests

3.1.1. Effect of Concrete-Filled Steel Tubes
Figure 3 shows the load and the mid-span deflection relationships under static loading tests. The CFST-type beams C1 and C2 show almost same load-deflection curves, and the RB-type beams D1 and D2 also do so. Therefore the experiments are reliable. Since both types of beams have been designed to have an equal ultimate bending strength, there is little difference of the ultimate strength between the two types. However there is a clear difference of the final deflection between the two types. This is due to the fact that the CFST improves the ductility capacity. Figure 4a shows the failure of specimens C1 and D1 at the mid-span. When the compression concrete is crushed heavily, the reinforcing bars of D1 buckle between the stirrups, followed by the decrease of the beam strength. Such a buckling mode does not appear in the case of the CFST-type, though a few circular holes of CFST are deformed to an ellipse. Thus the ductility improvement is achieved by using the CFST for the compression reinforcement.

The strength of the beam CN, in which the steel tubes without circular holes are used, is suddenly

decreased from 220 *kN* to 180 *kN*, when the mid-span deflection reaches to 22 *mm* (see Fig. 3). At this stage of loading, concrete cracks vertically on the compression side over the support, as shown in Fig. 4b(i). The CFST slides out as the mid-span deflection is increased as shown in Fig. 4b(ii). Comparing CN with C1 and C2, the circular holes made along the steel tube are clearly confirmed the formation of a series of concrete dowels which act in shear.

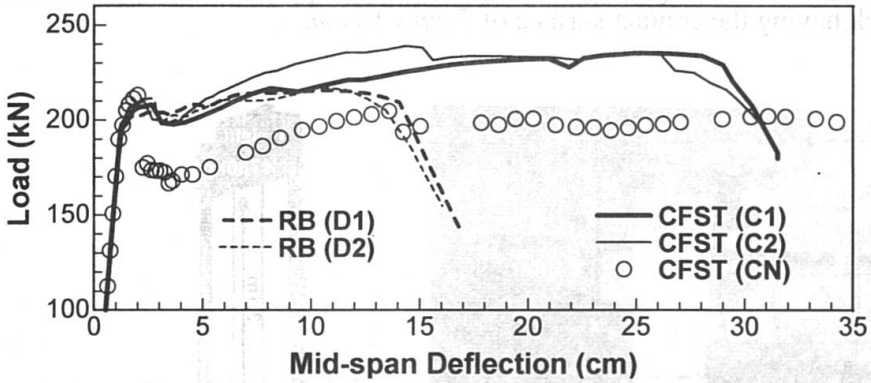

Fig. 3 Load-deflection curves (Improvement in ductility using CFST)

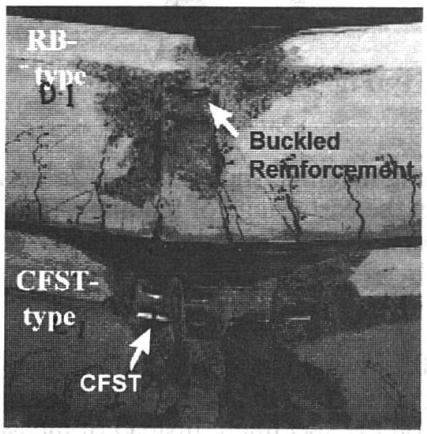

Fig. 4a CFST and buckled reinforcement

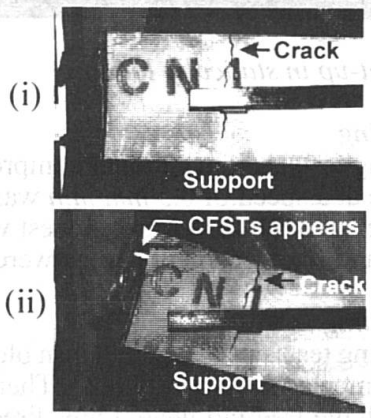

Fig. 4b Typical crack on CN

Specimen		Yield Deflection δ_Y (mm)	Ultimate Load P_U (kN)	Deflection at $0.95P_U$ δ_L (mm)	Ductility Factor δ_L/δ_Y	Energy Absorption E_n (kNm)
CFST Type	C1	17.5	235	292	16.7	64.2
	C2	15.4	238	278	18.1	61.4
	CN	16.4	213	340	20.7	65.2
RB Type	D1	18.5	217	143	7.7	29.2
	D2	15.0	217	132	8.8	26.7

Table 2 Ductility capacity in static loading tests

3.1.2. Bending Strength and Ductility Capacity

The experimentally observed ductility-factor for each beam and the relative values are summarized in Table 2, in which, δ_Y is the yield deflection when the strain at mid-span of tension reinforcement reaches the yield strain, P_U is the ultimate load, δ_L is the limit-state deflection when the load decreases to $0.95P_U$, δ_L/δ_Y is the ductility factor and E_n is the energy absorption capacity evaluated as the area below the load-deflection curve in Fig. 3. It is clear from Table 2 that the CFST-type beams exhibit the ductility factor and the energy absorption capacity more than two times as compared with the RB-type beams. The beam CN having the CFST without holes exhibits also an excellent ductility capacity, though the beam strength suddenly decreased after the peak load as shown in Fig. 3. This is due to the fact that in the case of the CFST without holes, the

bond-slip occurs along the whole surface of the CFST and the extreme crushing the CFST subjected to the bending moment does not appear. It can be concluded that the beam CN can absorb much energy, however, its use is not recommended due to sudden decrease in strength caused by bond-slip.

3.2 Impact Loading Tests

3.2.1. Impact Load - Time History

Figures 5(a) and 5(b) show the time history of the impact load and the weight displacement corresponding to the CFST-type (C3 & C4) and the RB-type (D3 & D4), respectively. A peak load, which is not shown in the figure, appears as an impulsive wave for an instant. Maybe, it has no effect on the beam strength. The results are reliable, because there is not any difference between C3 and C4 as well as between D3 and D4. The weight of 1780 *kg* and 3.1 *m* free-fall was incapable of breaking the beams C3 and C4 at one fall. On the other hand the beams D3 and D4 were crushed and touched the test-bed. These observations are indicated in Fig. 5(a) and 5(b) as "*rebound*" and "*crush & touch the test-bed*", respectively.

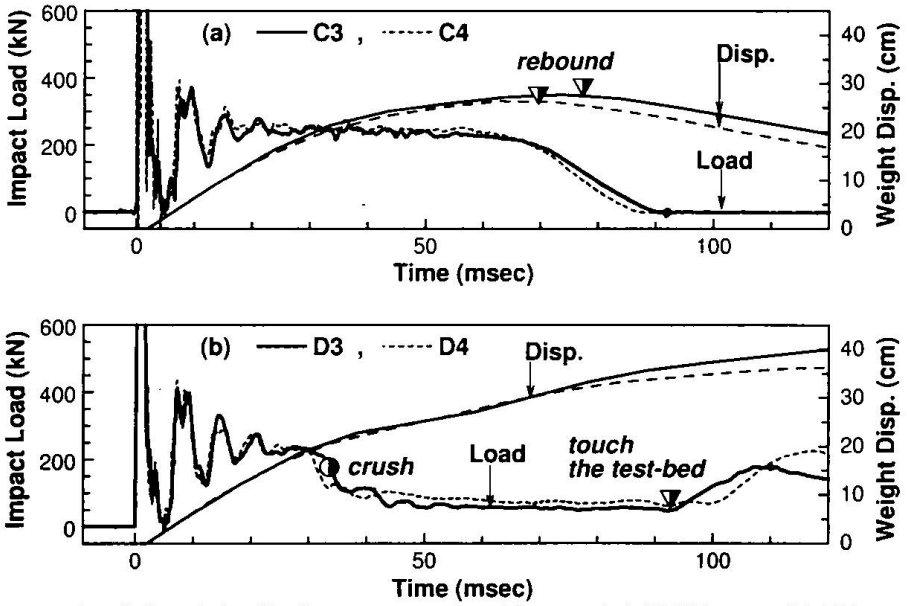

Fig. 5 Impact load & weight displacement -- time history: (a) CFST-type, (b) RB-type

3.2.2. Impact Load vs. Beam Response and Energy Absorption

The typical relations between the impact load and the weight displacement are shown, with a solid line, in Figs. 6(a) and 6(b). The energy absorption is also shown with a dashed curve. Furthermore the static load-deflection curves for C1 and D1 are also compared with the impact loading tests as shown in Fig. 6. Only for the CFST-type beam C4, the second fall of the weight from the height of 2.0 *m* was carried out, because the first fall did not cause heavy crush on the beam. In Fig. 6(a) the data due to the second fall are linked to that at the final beam displacement in the first fall, and are represented by a thin line and a thick line, respectively.

Even in the second fall the weight-rebound is seen in Fig. 6(a). This means that the beam, which is being in the limit state because of the considerable cracking, still has a little strength. The beam C4 has absorbed an energy of 81.4 *kNm* which is 1.3 times as large as that of the CFST-type beams tested statically. On the other hand, at the "crush" point in Fig. 6(b) the RB-type beam D4 has absorbed an energy of 41.9 *kNm* which is 1.5 times as large as that of the RB-type beams tested statically. The final beam-deflection due to an impact load is slightly larger than that in the static loading test, however there is little difference in the resistance strengths between the impact test and the static test when the impact loads are roughly averaged. Therefore the resistance strength and the energy absorption capacity of these beams can be estimated conservatively from the static test results.

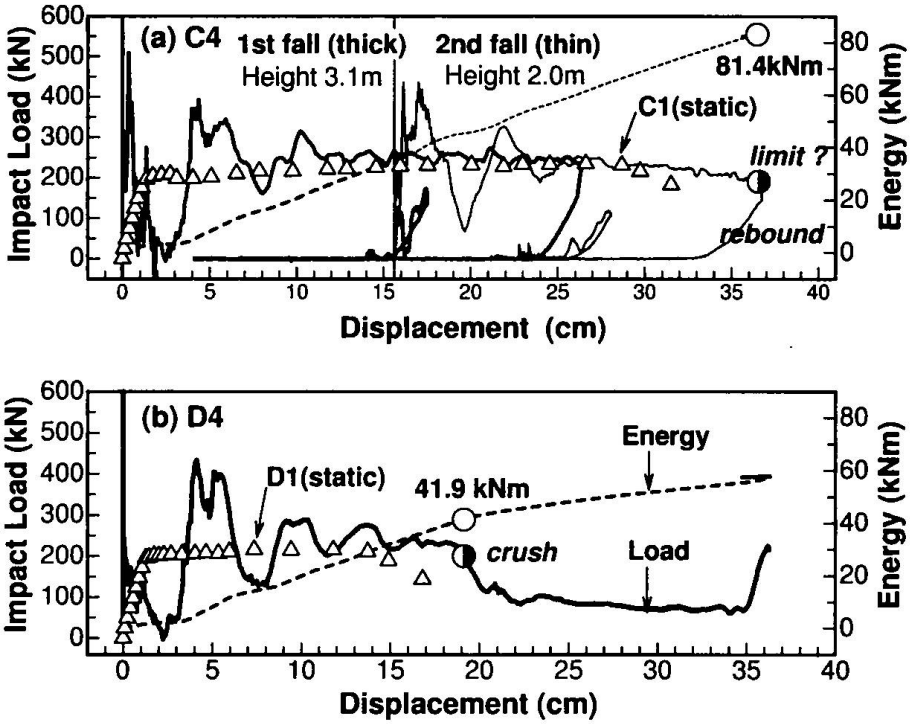

Fig. 6 Impact load and energy absorption -- weight displacement: (a) C4, (b) D4

4. Conclusion

The concrete-filled steel tubes (CFST) were employed as the compression reinforcement of RC-beams which are called CFST-type beams. These beams are expected to be used in rock-shed structures. A series of experiments was carried out with two types of the loading patterns, i.e., static load and impact load. It is shown that the CFST improves the ductility capacity and the energy absorption capacity more than two times as compared with the reinforcing bar commonly used for the RC-beams. The CFST is effective for reinforcing the RC-beams used in rock-shed structures in which the design should be based on the energy absorption concept.

5. Acknowledgment

The work presented in this paper was supported by Nippon Zenith Pipe Co.,Ltd. and Yoshida Advanced Designing Office.

6. References

[1] Yashiro H.: Transverse Reinforcement and Ductility of Reinforced Concrete Beam and Columns, Proc. of JCI Symposium on Design of Reinforcement and Ductility of Concrete Structures, JCI-C20, pp.125-130, 1990.

[2] Maegawa K., Kajikawa Y. and Yoshida H.: Bending Strength of Steel-Pipe Beams Filled with Concrete Reinforced by PC-Bars, Journal of Structural Engineering, Vol.39A, pp.153-164, 1993.

[3] Maegawa K. and Yoshida H.: Impulsive Loading Tests on Concrete-Filled Tubular Steel Beams Reinforced with Tendon, Journal of Structural Mechanics and Earthquake Engineering, No.513/I-31, pp.117-127, 1995.

Crack Formation in Bending Composite Elements

Bronius JONAITIS
Assoc. Prof. Dr.
Vilnius Gediminas TU
Vilnius, Lithuania

Bronius Jonaitis, born 1949
Dr. technical Sc. degree 1985
works at the department
of concrete structures.

Vytautas PAPINIGIS
Assoc. Prof. Dr.
Vilnius Gediminas TU
Vilnius, Lithuania

Vytautas Papinigis, born 1953
Dr. technical Sc. degree 1983
works at the department
of concrete structures.

Summary

The paper examines behaviour of composite structures, i. e. bending reinforced concrete elements, armoured externally under short - term static loadings the influence of external reinforcement and its anchorage towards resistance of crack formation, rigidity and strength has been analysed.

On the basis of the test results the methods for calculation of strength, cracking and rigidity have been compared.

1. Introduction

At present external glued reinforcement is widely used in the world for practical restoration of serviceability condition of structures. Strips or sheets of steel, glass fiber, asbestos cement are glued to the concrete surface of structures. Sheets and strips can be readily adjusted to various cross - sectional shapes, permanent load and depth of the structures practically are not increased, the job is quite simple and speedy.

External bonded reinforcement and the layer of polymer glue reduce concentration of stress in the tension zone, increase ultimate extensibility and tension strength of concrete, increase resistance to cracking and stiffness of members.

Resistance to cracking stiffnes and carrying capacity of flexural members with external reinforcement depend substantially on reliability of bond between concrete and external reinforcement. In the care of inadequate anchorage of the external reinforcement a crack may appear along the joint and consequently effect of external reinforcement reduces. Therefore it is essential to ensure reliability of bond between reinforcement and surface of the structure to be strengthened.

The best anchorage of glued reinforcement is achieved when this reinforcement is extended behind the supports. It is complicated to do so in strengthening of flexural members in service and it leads to the use of additional anchorage by the means of special anchors. It is associated with supplementary work and material expenditure. Thus the

problem of required length of extension of glued reinforcement behind the critical cross - section, i.e. determination of the development length is urgent.

This article deals with influence of external glued reinforcement on crackresistance and strength of normal sections of flexural members - beams.

2. Experimental investigations in members strengthened with glued external reinforcement

Behaviour of flexural members - strengthened with glued external reinforcement have been investigated in the department of reinforced concrete structures of Vilnius Gediminas technical university.

Four series of beams have been tested under short time static load. A series consisted of 2 beams. Beams tested were of 70×100 mm in cross - section and length of the beams was l=970 mm. The beams were made of normal weight concrete of cube strength $R_{15,m}$=41,5 MPa, reinforced with 2∅5 Bp I (reinforcement ratio μ_s=0,00696). In addition beams were reinforced with the following external glued reinforcement:

- non - metallic - 3 layer of glass fabric impregnated with epoxy resin paste (series S1 and S3);
- metallic - 0,72 mm thick steel strip of grade S_T 3 (series S2).

The external reinforcement of beams of series S3 were lapped over external ribs of the beams.

Diagrams of control beams S0 and those with glued external reinforcement S1, S2 and S3 are shown in Figure 1.

In beam tests moment of crack formation $M_{crc,obs}$, failure moment $M_{u,obs}$, distance between normal cracks and limit deformations of concrete in Tension zone were determined.

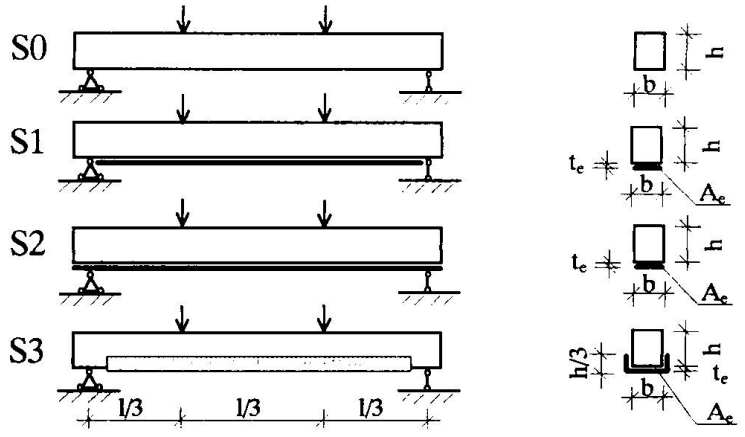

Fig. 1 Diagrams of reinforcing of beams with external glued reinforcement

The main characteristics of tested beams and the main test results are presented in Table1.

No of sample series	Cube strength of concrete in compression	External reinforcement				Test results			
		Type	Strength R_e, MPa	A_e, cm^2	$\varepsilon_{e,u}\times10^5$	$M_{crc,obs}$ kNm	$\frac{M_{crc,obs,i}}{M_{crc,obs,o}}$	$M_{u,obs}$ kNm	$\frac{M_{u,obs,i}}{M_{u,obs,o}}$
S0		–	–	–		0,39	1	2,05	1
S1		glass fabric	55,6	2,775 2,625	1013	0,78	2	2,77	1,35
S2	41,5	metal strip	R_y= =287,7	0,504	400	1,3	3,33	2,21	1,08
S3		glass fabric	76,48	3,85 2,56	963	0,78	2	2,78	1,35

Table 1 The main characteristics of samples and test results

According to the test results (see Table 1) resistance to normal crack formation of beams strengthened with external non - metallic and metallic glued reinforcement increased by 2 and 3,33 times, respectively, in comparison with control beams.

Many fine cracks appeared in beams strengthened with external reinforcement. Their width a_{crc}=0,025 - 0,05 mm and average spacing l_{crc}=55 - 60 mm. Crack width in non - strengthened (control) beams was larger a_{crc}=0,15 mm and spacing was l_{crc}=85 mm.

Strength of cross - section increased 1,35 and 1,08 times respectively. Lower increase in strength of cross - sections of beams strengthened with metallic external reinforcement is due to the fact, that the metallic reinforcement was not fully exploited, because of inadequate strength of joint between reinforcement and concrete surfaces, reinforcement at support regions broke off and the bond between reinforcement and concrete surfaces was damaged.

3. Calculation of crack formation moment

Resistance of crack formation of flexural members with glued external reinforcement may increase due stress redistribution between strengthening structure and external reinforcement and also due to increased extensibility limit of concrete layers saturated with glue. Efficiency of exploitation of external reinforcement depends on deformability (yielding) of links, the function of which is performed by glue seam. Results of calculation of crack formation moment depend on the accuracy of assesment of yielding in glue seam. Quite a few number of methods for calculation of cracking formation moments proposed by various authors are known. Some of them are analysed and calculation results compared below.

Crack formation moment in reference [1] is recommended to calculate as follows:

$$M_{crc} = \frac{W_{pl} \cdot R_{br} \cdot k_p}{\left[1 - \frac{k_z \cdot z \cdot (z+r)}{\gamma \cdot E_b \cdot I_{red}}\right]}, \quad (1)$$

where: k_p is a coefficient to allow for tensile strength of concrete covered by polymer, $k_z \leq 1$ and it is coefficient to account for deformability (yielding) of the links; z is distance between external reinforcement and the centroid of the cross - section, r=distance between the centroid of the cross - section and the upper kern point.

In reference [2] a general method for calculation of crack formation bending moments of flexural reinforced concrete members with additional external non - metallic reinforcement is proposed. A triangular stress diagram in concrete under compression is recommended by the authors for the case when compressive stress in the extreme compressive layer of the cross - section does not exceed the limit of microcracking of concrete, and in the opposite case this diagram is assumed to be trapezium. Then M_{crc} is calculated as follows:

$$M_{crc} = \frac{c \cdot R_{bt}}{h_t}\left(I_{b,el} + \alpha_s' \cdot I_s' + \alpha_p' \cdot I_s' + \alpha_s \cdot I_s + \alpha_e \cdot I_e\right) + R_{bt}\left(S_{bt} + \varphi \cdot S_{b,pl}\right) + P \cdot e_n, \quad (2)$$

where: $c=\varepsilon_{bt,u}/\varepsilon_{bt,el}$, I_s', I_p', I_p, I_s are second moments of area of cross - sections of adequate compressive and tensile reinforcing bars; I_e, $I_{b,el}$ are such moments but of external reinforcement and of concrete compression zone the depth of which is equals to $x(1 - \eta)$; $S_{b,pl}$ - the first moment of area of concrete compression zone the depth of which is ηx, S_{bt}=the same but for tension zone in depth of h_t ; P=concrete precompression force; e_n =distance from the point of application of force P up to the neutral axis; h_t=tension zone depth in a section with crack; coefficient $\varphi=\sigma_{b,max}/R_{bt}$; α=reinforcement to concrete modular ratio

The method of calculation of crack formation moment proposed in reference [3] also allows for plastic deformations of concrete in tension. the following formula is proposed for cracking moment calculation:

$$M_{crc} = \frac{\varepsilon_{btu}}{h - x}\left[\frac{E_{bk} \cdot b \cdot x^3}{2 + n_\sigma} + E_s \cdot A_s (h_0 - x)^2 + E_e \cdot b_e \cdot t_e (h - x)^2 + E_{btu}' \cdot \frac{b(h-x)^3}{2 + f_t}\right], \quad (3)$$

where: ε_{btu} is ultimate deformations of extreme fibers of concrete in tension; E_{bk} is deformation modulus of glues; E_{btu}' is the secant deformation modulus of tension concrete at failure; $f_t = E_b / E_{btu}'$ and is characteristic of non - linear behaviour of tension concrete.

Sample code	Method 1 [1]	Method 2 [2]	Method 3 [3]	Method 4 [4]
	$\frac{M_{crc,obs}}{M_{crc,cal}}$	$\frac{M_{crc,obs}}{M_{crc,cal}}$	$\frac{M_{crc,obs}}{M_{crc,cal}}$	$\frac{M_{crc,obs}}{M_{crc,cal}}$
S1-1	0,948	1,413	1,03	1,50
S1-2	0,929	1,376	1,03	1,469
S2-1	1,363	1,854	0,755	1,903
S2-2	1,30	1,774	0,748	1,823
S3-1	0,91	1,340	0,941	1,432
S3-2	0,908	1,340	0,948	1,432
Bondarenko V.M. [3]	0,997	1,541	1,03	1,657
	1,144	1,10	1,05	1,937
	1,176	1,894	1,054	2,044
	0.858	1,217	1,08	1,315
	0,970	1,395	1,071	1,508
	1,060	1,538	1,084	1,666
Voronkov R. V [6]	0,993	0,719	-	1,33
	1,03	0,745	-	1,63
	1,00	0,730	-	1,33
	0,719	0,615	-	1,11
	1,09	0,759	-	1,01
	1,189	0,922	-	0,835
	1,2	0,931	-	0,835
*	0,832	1,214	-	1,324
*	0,894	1,39	-	1,518
*	1,142	1,649	-	1,795

* The beams tested at reinforced concrete department of VGTU

Table 2 Results of calculation of crack formation moments M_{crc}

Calculation methods	Number of samples	The mean value γ_m	Standard deviation S_γ	Coefficient of variation δ_γ	k_{min}, at $\beta=2$
1	22	1,03	0,158	0,153	1,4
2	22	1,248	0,388	0,311	2,12
3	12	0,985	0,118	0,12	1,34
4	22	1,47	0,33	0,225	1,24

Table 3 Results of statistical analysis of ratio $\gamma=M_{crc,obs}/M_{crc,cal}$ *moments of crack formation*

Values of crack formation moments are calculated according the methods discussed and compared with test results on beams. Results of comparison are presented in Tables 2 and 3. The average value of ratio at crack formation moments $\gamma_m = M_{crc,obs}/M_{crc,cal}$ characterizes accuracy of method of calculation, while the average square standard deviation of this ratio S_γ and coefficient of variation δ_γ define reliability of the method (see Table 3). It was assessed by verification that distribution of the ratio $\gamma = M_{crc,obs}/M_{crc,cal}$ agrees with the normal law of distribution. Then according to [5] the minimum conventional reliability coefficient k_{min} of a calculation method can be determined:

$$k_{min} = 1/\gamma_m(1-\delta_\gamma \cdot \beta) \qquad (4)$$

where: β is number of standard deviations in accordance with assumed reliability.

The minimum conventional reliability coefficient k_{min} of calculation method makes a part of general safety coefficient. Its values are presented in Table 3.

After comparing results of analysis presented in Table 3 it is easy to discover, that calculation methods 1 and 3 can give quite accurate and sufficiently reliable results of calculation of normal crack formation moments of beams strengthened with external glued reinforcement.

References

1. Kamaitis Z. Vostanovlenie usilenije konstrukcij i sooruzhenij sintetytsheskimi smolami. - Vilnius. Technika, 1992. - 280 p.

2. Valivonis J., Jurksha A. Obobshchionyj metod raszheta izgibajemych zhelezobetonnych elementov s dopolnytelnym wneshnym nemetalitsheskim armirovanijem. Trudy VTU "Zhelezobetonnyje konstrukciji", 1995, № 17. - p 43 - 48.

3. Bondarenko V. M., Schagin A. L. Raschiot efektivnych mnogokomponentnych konstrukcij. - M.: Strojizdat, 1987. - 176 p.

4. Posobje po projektirovaniju betonnych i zhelezobetonnych konstrukcij iz tiazhiolych i liogkoch betonow bez predvaritelnogo napriazhenija armatury (k SNiP 2.03.01 - 84). - M.: Strojizdat, 1986.

5. Vadlūga R. R., Kudzis A.P. Analiz tochnosti i nadiozhnosti raschiota po prochnosti izgibajemych zhelezobetonnych elementow kolcewogo setchenija. Trudy VISI, "Zhelezobetonnyje konstrukciji", Vilnius 1976, № 7, p 155 - 162.

6. Voronkov R. V. Zhelezobetonnyje konstrukciji s listowoj armaturoi. L.: Strojizdat, 1975. - 145 p.

Shear Resistance of Stud Connectors with Profiled Steel Sheeting

Xiamin HU
Assoc. Prof.
Nanjing Arch. & Civil Inst.
Nanjing , China

Xiamin Hu, born 1958, Associate Professor at Nanjing Architectural Civil Engineering Institute. His research interests include composite structures reinforced, concrete structures and neural networks.

Chengjian WEI
Assoc. Prof.
Nanjing Arch. & Civil Inst.
Nanjing China

Chengjian Wei , born 1957, Associate Professor at Nanjing Architectural Civil Engineering Institute. His interests include neural networks, evolutionary computation, fuzzy system and artificial life

Rongfei ZHAO
Engineer
Nanjing Arch.& Civil Inst
Nanjing China

Rongfei Zhao , born 1968, Computer Engineer at Nanjing Architectural Civil Engineering Institute. His interests include neural networks , evolutionary computation, fuzzy system and artificial life

Summary

In this paper, based on the backpropagation model of neural networks, the details of the neural network methodology are presented to predict ultimate shear resistance of stud connectors with profiled steel sheeting. The analysed results show that the neural network predictions have a better agreement with the experimental data of the push-out tests than the predictions using other conventional methods.

1. Introduction

The use of mechanical shear connectors is essential for ensuring composite action in the composite beams. The head stud is the most widely used type of connector in composite construction, especially in composite floors system with profiled steel sheeting. The direct shear strength of connectors may be evaluated by using a representative model test known as the push out test (Fig. 1). In the last two decades years many researchers have conducted the push-out test on studs with profiled steel sheeting and found that specimens that included the profiled steel sheeting reduced both the strength and stiffness of the connection. But since the structural behavior of the stud connectors with profiled steel sheeting is quite complicated and not amenable to simple calculations, until now no accepted calculation model has been developed to predict the shear strength resistance of stud connectors with profiled steel sheeting.

This paper investigates the feasibility of using neural networks to evaluate the ultimate shear strength of stud connectors with profiled steel sheeting. A neural network is an information processing system that essentially mimics the structure and function of the brain. The neural networks are particularly useful for evaluating systems with a multitude of nonlinear variables, but no predefined mathematical relationship between the variables is given. In this paper, based on the backpropagation model of neural networks, details of the neural network methodology are presented to predict ultimate shear resistance of stud connectors with profiled steel sheeting. Where the compressive strength and modulus of the concrete, the tensile strength of the stud material, the size of the stud, the geometry of the profiled sheeting are chosen as the critical factors of the nonlinear variables. The analysed results show that the neural network predictions have a better agreement with the experimental data of the push out tests than the predictions using other conventional methods.

2 Neural Networks

Neural networks are computational models of many nonlinear processing element arranged in patterns similar to biological neuron networks. A typical neural network has an activation value associated with each node and a weight value associated with each connection. An activation function governs the firing of nodes and the propagation of data through network connection in massive parallelism. The network can be learned with examples through connection weight adjustment.

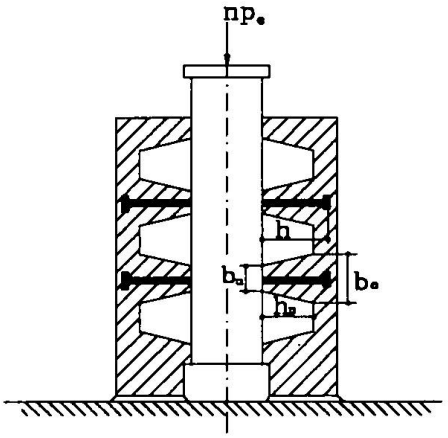

Fig.1 Push-out test

2.1 The computational model of neuron

McCllock and Pitts[1] proposed a binary threshold unit as a computational model for an artificial neuron. This mathematical neuron computes a weighted sum of its n inputs signals, x_j $j=1,2,...n$, and generates an output of 1 if this sum is above a certain threshold u. Otherwise, an output of 0 results. Mathematically

$$y = f\left(\sum_{j=1}^{n} w_j x_j - u\right)$$

where f(.) is a unit step function, and w_j is the synapse weight associated with the jth input

Using sigmoid function replace the Mccllock-Pitts neuron's threshold we get a generalized neuron model. The sigmoid function is a strictly increasing function that exhibits smoothness and has the desired asymptotic properties. The standard sigmoid function is the logistic function, defined by

$$g(x) = 1/(1+\exp(-\beta x))$$

where β is the slope parameter. The computational model of neuron is illustrated in Fig 2.

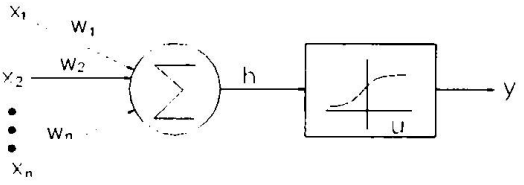

Fig. 2 Model of neuron

2.2 Network Architectures and Learning

Neural networks can be viewed as weighted directed graphs in which artificial neurons are nodes and directed edges are connections between neuron outputs and neuron inputs. Based on the connection pattern, neural networks can be grouped into two categories

- feed -forward network, in which graphs have no loops, and
- recurrent networks, in which loops occur because of feedback connection

A learning process in the neural networks context can be viewed as the problem of updating network architecture and connection weights so that a network can efficiently perform a specific task. The network usually must learn the connection weights from available learning patterns.

2.3 Multilayer feed-forward networks

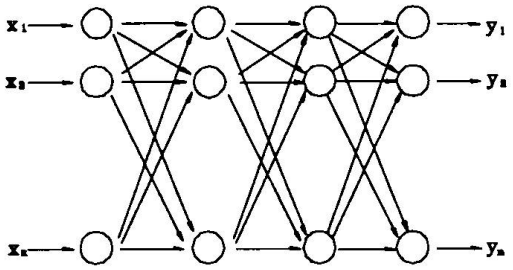

Fig. 3 Typical tree-layer perceptron

Fig. 3 shows a typical three-layer perceptron. In general a standard L_layer feed-forward network consists of an input stage, (L-1) hidden layers, and an output layer of units successively connected fully in a feed-forward fashion with no connections between units in the same layer and no feedback connections between layers.

The most popular class of multilayer feed-forward networks is multiplier perceptions in which each computational unit employs the sigmoid function. The development of the backpropagation learning algorithm for determining weights is a multilayer perceptron has made these networks the most popular among researchers and users of neural networks. The backpropagation learning algorithm is an iterative gradient algorithm designed to minimize the mean square error between the actual output of a multilayer feed-forward perceptron and the desired output. It requires continuous differentiable nonlinearities.

The BackPropagation Learning Algorithm as follows:

step 1 Initialized weights and offsets
set all weights and node offsets to small random values.
step 2 Present Input and Desired outputs
present a continuous valued input vector $x_1, x_2, \cdots x_n$ and
specify the desired outputs $d_1, d_2, \cdots, d_m$
step 3 Calculate Actual Outputs
use the sigmoid function to calculate outputs $y_1, y_2, \cdots, y_m$
step 4 Adapt weights
Use a recursive algorithm starting at the output node and working back to the first hidden layer. Adjust weights by

$$w_{ij}(t+1) = w_{ij}(t) + \eta \delta_j x_i' + \alpha(w_{ij}(t) - w_{ij}(t-1))$$

where $0 < \alpha < 1$, w_{ij} is the weight from hidden node i or from an input node to node j at time t, x_i' is either the output of node i or is a an input, η is a gain term, and δ_j is and error term from node j, if node is an output node then

$$\delta_j = y_j(1-y_j)(d_j - y_j)$$

where d_j is the desired output of node j and y_j the actual output.
if node j is an internal hidden node, then

$$\delta_j = x_j'(1-x_j')\sum_k \delta_k w_{jk}$$

where k is over all nodes in the layers above node j, internal node thresholds are adapted in a similar manner by assuming they are connection weights on links from auxiliary constraint-valued inputs.
step 5 Repeat by going to step 2

3. Prediction of the shear resistance

3.1 Learning of the neural network

A total of 65 push-out test specimens reported by Bode and Hu [2] are used here to demonstrate the performance of the backpropagation model in the prediction of the shear resistance of stud connectors with profiled steel sheeting. All these tests were carried out in Gemany and originally reported by Roik and Buehrkner [3,4], Roik and Lungeshausen [5], Bode and Kuenzel [6,7] ,Roik and Hanswille[8].In these tests the holes were cut out in the decking and the stud connectors were welded through the holes to the beam beneath. For a given geometric configuration of a stud with profiled stud sheeting, the ultimate shear strength of the connection P depends on the strength and the size of the stud, on the strength and the stiffness of the concrete, on the geometry of the profiled steel sheeting and on the number of studs per rib. Therefore the following expression is gotten:

$$Mapping \quad T: f(f_c', E_c, f_u, d, h\text{-}h_p, h_p, b_u, b_o, N_r) \rightarrow P$$

where f_c' and E_c represent the compressive strength and modulus of the concrete, f_u is the tensile strength of the stud material, d is the diameter of the shank of the stud, h is the height of the stud. h_p is the over depth of the profiled sheeting. b_u and b_o represent the bottom width and top width of the profiled sheeting, N_r is the number of studs per rib.

Learning of the neural network is essentially carried out through the presentation of a series of example patterns of associated input and observed output values,and some preprocessing of the data is usually required before presenting the input patterns to the neural network. This usually involves scaling or normalization of the input patterns to values in the range 0-1. In this study, the learning example patterns consisted of 40 typical push-out test specimens collected by Bode and Hu[2] .

The neural network learned is constructed here with nine-nods in input layer, seventeen-nods in first hidden layer, twelve-nods in second hidden layer , fifteen-nods in third hidden layer and one node in output layer. η and α are taken as 0.5 and 0.4. The following expression was used to normalize data

$$Normalized\ value = \frac{Actualvalue - Minimumvalue}{Maximumvalue - Minimumvalue}$$

Learning is carried out iteratively until the average sum squared errors over all learning patterns are minimized based on the above backpropagation model .This occurred after about 1552 cycles of learning.

3.2. Comparison of predicted values with experimental data

On the satisfactory completion of the learning phase, verification of the performance of the neural network is then carried out using patterns that were not included in the learning set. Push-out test specimens that only broadly resemble the data in the learning set were used to verify whether the neural network can generalize correct responses. Details of the testing pattern and the neural network predictions are summarized in table 1. A comparison of the predicted values P_p and experimental values P_e indicate that the neural network is capable of generalization and gave reasonable predictions. Using the ratio of experimental data to neural network predictions as an indicator, the mean and standard deviation of this ratio for the 25 specimens are 1.04 and 0.069, respectively, as shown in table 1.

Prediction using the expressions of Bode and Hu[2] and the expressions of Roik and Lungeshousen[9] were also carried out to compare with the neural network approaches. The average of experimental shear strength to predicted strength ratios given by Bode and Hu's expressions and Roik and Lungeshausen's expressions are 1.06 and 1.07 ,while the corresponding standard deviations are 0.073 and 0.131, respectively. The coefficients of correlation of experimental versus predicted results are 0.976 (neural network approach), 0.975 (Bode and Hu's expressions), and 0.951(Roik and Lungeshausen's expressions). This indicates that the neural network approach is more reliable than the conventional methods.

It is to be noted that EC4 methods were here not compared because the equations in EC4 are not suitable for the predictions of stud connectors with pre-punched decking[2].

4. Conclusions

In this paper, a neural network for prediction of ultimate shear strength of stud connectors with profiled steel sheeting is presented. The study has demonstrated that the neural network can

Table 1 Comparison of Experimental Shear Strength P_e to Predicted Shear Strength P_p

Specimen	P_e,kN	Bode and Hu		Roik and lungeshausen		Neural Network		reference
		P_p,kN	P_e/P_p	P_p,kN	P_e/P_p	P_p,kN	P_e/P_p	
7.1	74.0	75.71	0.99	76.56	0.97	72.28	1.02	3
7.2	78.0	75.71	1.03	76.56	1.02	72.28	1.08	3
2.1	44.5	39.93	1.12	41.22	1.08	41.84	1.08	4
2.2	38.0	39.93	0.95	41.22	0.92	41.84	0.92	4
3.1	82.0	76.89	1.07	68.86	1.19	77.65	1.06	4
3.2	78.5	76.89	1.02	68.86	1.14	77.65	1.01	4
5.1	42.0	39.09	1.07	37.71	1.11	41.30	1.02	4
5.2	49.0	39.09	1.25	37.71	1.30	41.30	1.19	4
8.1	79.0	73.09	1.08	62.66	1.26	75.84	1.04	4
8.2	85	73.09	1.16	62.66	1.36	75.84	1.12	4
11.1	84.5	76.89	1.10	68.86	1.23	76.93	1.06	4
11.2	85.0	76.89	1.11	68.86	1.23	76.93	1.07	4
SH0-1	75.5	78.81	0.96	80.63	0.94	76.32	0.99	6
CS0-1	77.1	78.95	0.98	85.04	0.91	82.60	0.93	6
H1	114.0	111.65	1.02	118.14	0.97	111.35	1.02	7
H2	107.0	111.65	0.96	118.14	0.91	111.35	0.96	7
H3	114.0	111.65	1.02	118.14	0.97	111.32	1.02	7
H4	130.0	111.65	1.16	118.14	1.10	111.32	1.17	7
H5	111.0	111.65	0.99	118.14	0.94	111.35	1.00	7
H6	115.0	111.65	1.03	118.14	0.97	111.35	1.03	7
H7	122.0	111.65	1.09	118.14	1.03	111.31	1.10	7
H8	123.0	111.65	1.10	118.14	1.04	111.31	1.11	7
D1	107.0	96.8	1.11	101.94	1.05	104.47	1.02	8
D2	96.5	96.8	1.00	101.94	0.95	104.47	0.92	8
D3	106.0	96.8	1.10	101.94	1.04	104.47	1.01	8
mean			1.06		1.07		1.04	
Standard deviation			0.073		0.131		0.069	

effectively generalize correct responses that only broadly resemble the data tin the learning set. The predictions should be reliable, provided the input values are with the range used in the learning set. As new data becomes available, the neural network models can be learned readily with patterns that include these new data. The analyzed results indicate that the neural network has powerful capacity of dealing with inherent noisy or imprecise data. The neural network model was found to be more reliable than other conventional methods.

References

[1] Richard P. L.: An introduction to computing with neural nets. IEEE ASSP , 1987(4): 4-22

[2] Bode H.; Hu Xiamin: Untersuchungen zur Schubtragfaehigkeit von Kopfbolzenduebeln. Forschungsbericht, Universitaet Kaiserslautern, August 1993

[3] Roik, K.; Buerkner,K-E.: Beitrag zur Tragfaehigkeit von Kopfbolzenduebeln in Verbundtraegern mit Stahlprofilblechen. Der Bauingenieur 56,S. 97-110,1981

[4] Roik,K.; Buerkner,K-E.: Untersuchungen des Tragerverbundes unterverwendung von Stahltrapezprofilen mit einer Hoehe >80mm. Studiengesellschaft fuer anwendungstechnik von Eisen und Stahl e. V., Projekt 40 ,Duesseldorf,1980

[5] Roik,K.; Lungershausen,H.: Verbundtraeger mit Stahltrapezprofilblechen mit Rippenhoehe >80mm. Studiengesellschaft fuer Anwendungstechnik von Eisen und Stahl e.V.,Projekt 99,Duesseldorf ,1988

[6] Bode, H.; Kuenzel, R.:Zur Anwendung der Durchschweißtechnik im Verbundbau. Forschungsbericht 2/1991,Universitaet Kaiserslautern, Maerz 1991

[7] Bode,H.; Kuenzel,R.: Steifigkeit und Verformbarkeit von Vermitteln in Hochbau. International Symposium, Composite Steel Concrete Structures, vol.I Bratislava 132/1987

[8] Roik, K.; Hanswille, G.: Gutachten fuer die Holorib GmbH zur Frage der Tragfaehigkeit von Kopfbolzenduebeln bei auf dem Verbundtraegerobergurt gestobenen Profilblechen. Bochum,Juli 1988

[9] Roik,K.; Lungeshausen,H.: Zur Tragfaehigkeit von Kopfbolzenduebeln in Verbundtraegern mit unterbrochener Verbundfuge (Trapezprofildecken); Der Stahlban, H.58,1989,S.269-273

The Influence of Slab Bending Moments on the Load Bearing Behaviour of Headed Studs

Wieland RAMM
Prof. Dr.-Ing.
University of Kaiserslautern
Kaiserslautern, Germany

Wieland Ramm, born 1937, received his civil engineering degree and Ph.D. at TH Darmstadt.

Franz-Michael JENISCH
Dipl.-Ing., Research Assistant
University of Kaiserslautern
Kaiserslautern, Germany

Franz-Michael Jenisch, born 1962, received his civil engineering degree at TH Darmstadt. Since 1991 he has

Summary

The results of push-out tests, carried out with stud shear connectors and with simultaneously acting slab bending moments, are presented. The influence of the slab bending moments on the load-carrying capacity of the studs is described by means of interaction curves. The effect of varied ratios of transverse reinforcement and of sheet geometry is pointed out this way. Models that describe the transfer of stud shear forces in profiled concrete flanges are shown.

1. Introduction

The problems of longitudinal shear and simultaneously acting slab bending moments in the concrete flanges of composite beams were investigated in a project of a research group 'composite action' at the University of Kaiserslautern. In the scope of this project sixteen full-scale beam tests were carried out. The results of these tests were presented in detail in [5] and [6]. In the tests with composite beams in sagging moment regions an influence of the transverse slab bending moments on the load bearing behaviour of the beams was observed. In these beam tests smaller as well as higher ultimate loads occur in connection with smaller and higher slab bending moments. On one hand this influence can be caused by changes in the load-slip-behaviour of stud shear connectors as result of the simultaneously acting slab bending moments. On the other hand this effect can be caused by the influence of the transfer of stud shear forces on the load-bearing behaviour of the composite slab.

Figures 1 to 6 separately demonstrate the different stress effects acting together in the small area of concrete flange above the steel girder. Hereof figs. 3 to 5 show different truss-models, that describe the transfer of the stud shear forces from the bottom areas of the studs to the concrete plate above the sheets.
The transverse tensile forces created by the spreading of the compression forces of the longitudinal shear are shown in fig. 1. These tensile forces were described in detail by different authors, too, for example by Johnson et al. [3]. As shown in the picture shows a distribution of these tensile forces is possible among the reinforcement (T_{reinf}) and the profiled sheet (T_{sheet}) in the case of sheets with composite action.

Finally the internal forces in the profiled sheet and in the reinforcement due to the slab bending moments are plotted in fig. 2. In the lower regions of the ribs compression forces act in the sheets (C_{sheet}) and in the encased concrete (C_c). These compression forces will have effects on the load-

carrying capacity of the studs. Tensile forces act in the upper regions of the sheet (T_{sheet}) and in the reinforcement (T_{reinf}). They lead to cracks at the upper side of the slab. These cracks influence the load carrying capacity of the studs, too.

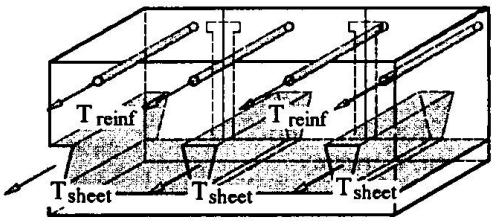

Fig 1: Tensile forces due to the longitudinal shear

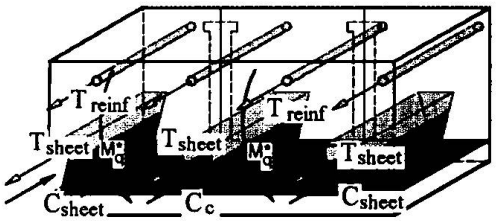

Fig 2: Internal forces as a result of the slab bending moments M_q^*

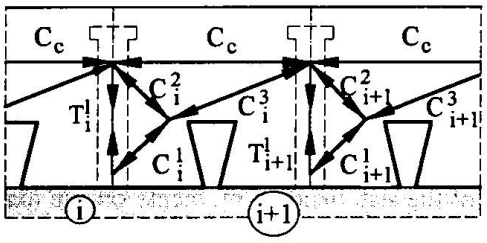

Fig 3: Truss-model for direct transfer of stud forces

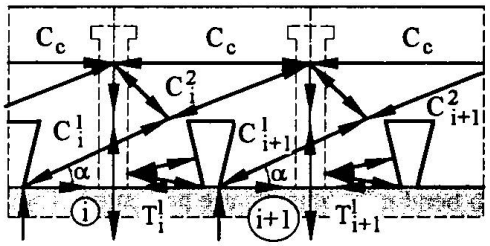

Fig 4: Truss-model for indirect transfer of stud forces (1. alternative)

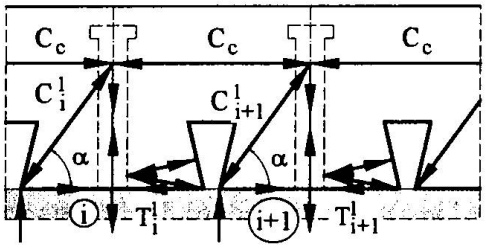

Fig 5: Truss-model for indirect transfer of stud forces (2. alternative)

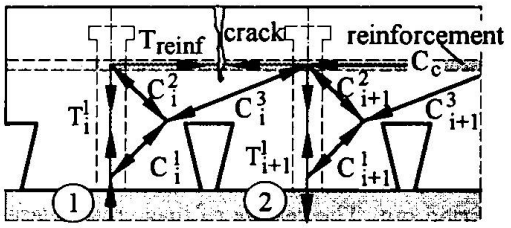

Fig 6: Truss-model for direct transfer of stud forces for the last stud of a beam

The figs. 3 to 5 demonstrate, that different models basing upon the truss-model theory can be used to describe the transfer of stud shear forces in profiled concrete flanges of composite beams. Figure 3 gives a model for a 'direct' transfer of the stud shear forces. This model does not consider possible tensile forces in the sheet. For the situation of the first stud at a beam or in push-out tests with two studs, see fig 6, transverse cracks occur in the upper region of the concrete flange due to tensile forces between the studs. In fig. 4 and 5 models for an 'indirect' transfer of the stud shear forces are plotted. In these models the profiled sheet is used in transmitting the stud forces to the concrete above the sheets. In reality all three models are acting together in transferring the stud shear forces. Because of this there are tensile forces in the sheets, described in the models of fig. 4 and 5 as well as transverse cracks between the studs, described in the model of fig 6.

More information about this transfer of stud shear forces and the influence of the transverse slab bending moments on this transfer was needed for the analysis of composite beams, especially for the investigation of the interaction of slab bending moments and longitudinal shear in the concrete flanges.

First sporadic push-out tests with simultaneous slab bending moments carried out by Bode and Künzel [1,2] and Lloyd and Wright [4] have also shown the above mentioned influence of the slab

bending moments on the load-bearing behaviour of the studs. Therefore additional and more detailed examinations about these problems were required.

2. Test Arrangement of Push-out Tests

Figures 7 and 8 show the test arrangement for the carried out push-out tests. Two independent loads were applied. The first load caused shear forces in the steel-concrete interface, the second load produced simultaneously and independently acting slab bending moments.

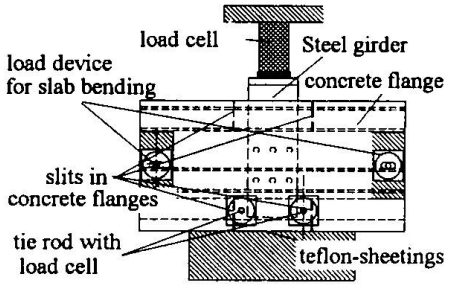

Fig 7: Test set-up and test specimen for push-out tests

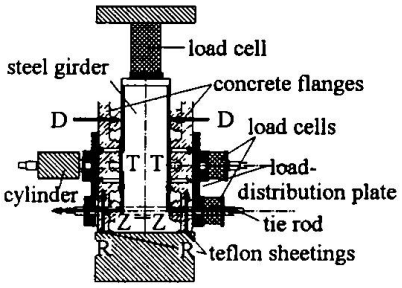

Fig. 8: Sectional view of test set-up and specimen for push-out tests.

Different ratios of slab bending moments and stud shear forces were examined with constant test parameters for the rest to determine interaction curves. For this purpose, load conditions defined in figs. 9 to 12 with the points A to G were tested.

The ribs without studs were slit to obtain clearly defined constant bending moments in the ribs with stud shear connectors. The test specimens were based on teflon sheetings to minimise the friction between the support and the test specimens.

The separation of the concrete flanges from the steel girder in the bottom regions of the specimens was prevented by using tie rods. With a load cell at each tie rod, the forces in the rod were measured.

In all tests the strains were measured at the transverse reinforcement, at two stud shear connectors, at one rib of the profiled sheet in one direction and at an other rib in three directions. With both flanges the slip between the steel girder and the profiled sheet, the middle of concrete above the sheets and the surface of the concrete flange was measured.

Tests were carried out with two extremely different types of profiled sheets. First SUPERHOLORIB 51 sheets with a wide and low rib were used. Secondly COFRASTRA 70 sheets with a narrow and high rib were tested. Both types of sheets had holes for stud shear connectors and were 0,88 mm thick.

Three series with SUPERHOLORIB 51 sheets each including seven push-out tests and one series with COFRASTRA 70 sheets including five tests of the wide range of 48 totally planned tests, have been carried out already. The different types of profiled sheets were examined in these tests with one and the same cross-section area of transverse reinforcement and in varying the slab bending moments.

3. Test results

In the following some selected results are presented about the influence of cross section area of the reinforcement and of the sheet geometry on the interaction between the slab bending moments and the load carrying capacity of stud shear connectors. Further results are shown to verify the described above truss-models.

The figures 9 to 12 show two interaction curves where related loads P^m of studs are plotted versus related bending moments of the slabs. Stud loads P^m are related to the bearing capacity P of the studs without slab bending moments, bending moments of the slab are related to ultimate bending moment with out stud forces. The first curve gives the yield loads P_y^m of the studs. In this case the yield load of the stud is defined as the smaller value of the maximum load multiplicated with 0.9 and the minimum load $P^m_{Ru,10mm}$ reached up to a slip of 10 mm. Therefore this curve is relevant for the design of composite beams. The second curve gives the maximum load reached up to a slip of 10 mm. It is needed for an exact calculation of composite beams for example with FEM. These two interaction curves were plotted for three series of tests with SUPERHOLORIB 51 sheets and one interaction curve for the series of COFRASTRA 70 sheets.

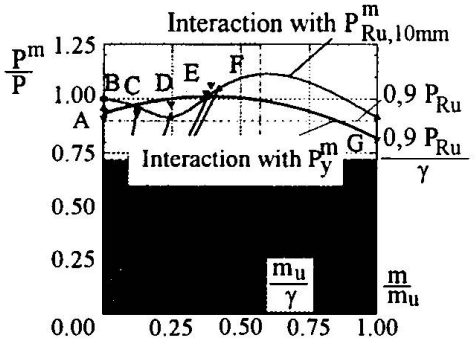

Fig. 9: Interaction curves of tests of series HOL339

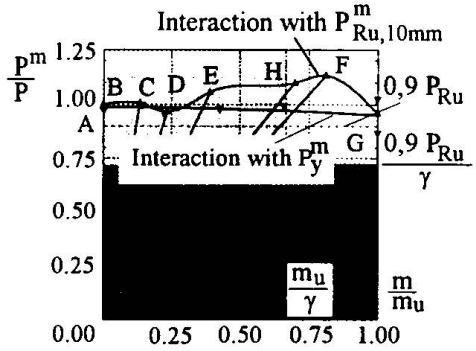

Fig. 10: Interaction curves of tests of series HOL785

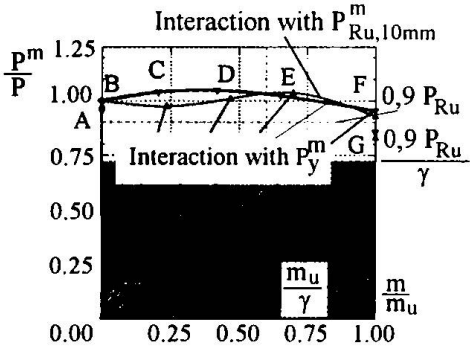

Fig. 11: Interaction curves of tests of series HOL1589

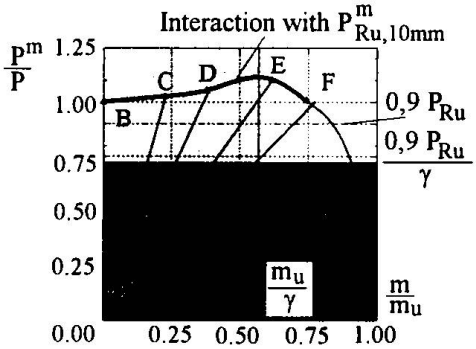

Fig. 12: Interaction curves of tests of series COF785

The mentioned figures show no change in yield loads by small slab bending moments in the tests of series HOL339 ($A_s = 7{,}85$ cm^2 of transverse reinforcement, fig. 9) and of series HOL785 ($A_s = 7{,}85$ cm^2, fig. 10). In the tests of series HOL1589 ($A_s = 15{,}89$ cm^2, fig. 11) there was a small increase of yield load by small slab bending moments. With high slab bending moments a decrease was observed in all series. The magnitude of the decrease of yield loads depends on the ratio of reinforcement. The tests of series HOL339 show the largest and the tests of HOL1589 the smallest decrease. In all tests the ultimate load of the studs exceeded the design loads of studs without slab bending, obtained from test B ($\frac{0{,}9 * P_{Ru}}{\gamma}$).

Comparing the maximum loads reached up to a slip of 10 mm different curves of interaction were observed, too. In all tests there was a decrease of the load-carrying capacity of the studs by small

slab bending moments and an increase with higher slab bending moments. The effect of slab-bending moments depends on the ratio of transverse reinforcement too.

The comparison of tests with SUPERHOLORIB sheets (fig. 9 to 11) with the first tests series with COFRASTRA 70 sheets (fig. 12) demonstrates the influence of the rib geometry. In this figure only maximum loads are plotted, as they were reached nearby 3 mm slip, as loads decreased afterwards. In these tests an increasing of the ultimate loads of studs with increasing of slab bending moment and an estimated decrease of load carrying capacity with higher slab bending moments. This decrease has a greater influence on load bearing behaviour of studs than in tests with SUPERHOLORIB sheets. Further tests will give more detailed information about this problem.

This load-bearing behaviour of the studs is a result of compression stresses in the bottom region with small slab bending moments, and of wide longitudinal cracks with high slab bending moments. For more information about this problem see [5,6].

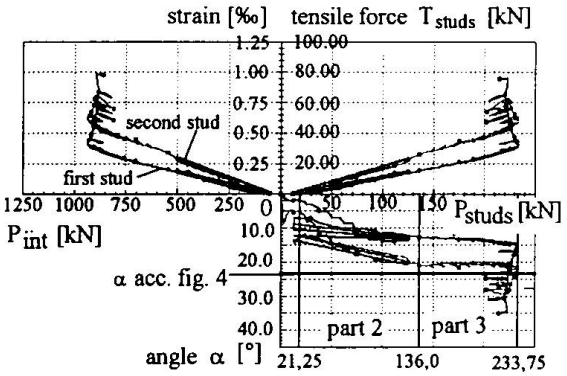

Fig. 13: Strain, tensile force in stud shear connectors and angle α of a test with free possible separation between slab and steel girder

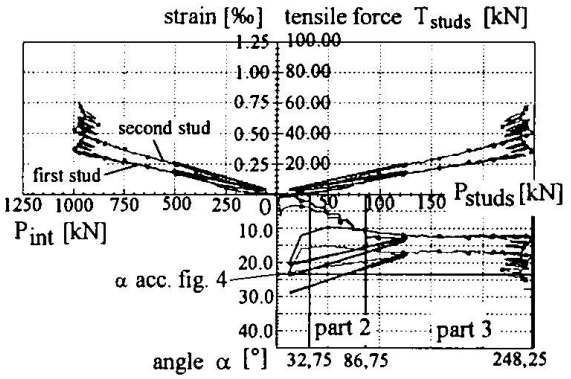

Fig. 14: Strain, tensile force in stud shear connectors and angle α of a test with hindered separation between slab and steel girder

In figures 13 and 14 the measured strains of the stud shear connectors are plotted for two studs obtained from a test with free possible separation of the concrete flange from the steel girder and a test with hindered separation but with slab bending. In the upper left part of the pictures the strains measured at the lower and the upper stud are plotted versus the load in the interfaces P_{Int} between the steel girder and the profiled flange. In the upper right part the calculated tensile forces T_{stud} in the group of two studs are plotted versus the shear force P_{studs} of the group. Finally in the lower right part the calculated angle α of the compression forces of the in fig. 4 described truss model are plotted versus the shear force of the group of two studs.

The comparison of these pictures shows common effects in both tests. On one side the strains and tensile forces increase linearly with growing force in the interface between steel and concrete up to the maximum load reached up to a slip of 10 mm. Thereafter the strain increases without an increase of the stud shear forces. On the other side the curve of the calculated angles α of the compression force can be divided in three parts. Part one is a horizontal line at small stud shear forces, which can be described as a uncracked situation of transfer of stud shear forces. Part two shows increasing angles α with increasing stud shear forces. In this part the cracks occur in the concrete flanges. In part three the calculated angle α has a constant value up to the maximum load reached up to 10 mm slip. Beyond this point the angle increases without an increasing of stud shear forces.

The transverse crack described in fig. 6 occured in all push-out tests at a load range corresponding to part two. Further the strain measured in the lower stud was greater than in the upper stud. This corresponds to the truss-model described in fig. 3. According this model higher tensile forces can be calculated in the second stud (lower stud in the push-out tests). Different from this model but in accordance with the other models described in figure 4 and 5 tensile strains were observed in upper flange of the sheets. These strains that occur between the studs and beside the steel girders are influenced by the slab bending moments. Furthermore the principal strains are also influenced by the slab bending moments. As a consequence it can be said that both models of 'direct' and 'indirect' transfer of stud shear forces act simultaneously.

Finally it should be mentioned, that the slab bending moments have an influence on the stiffness of the interface between steel girder and concrete flange, too. More detailed information will be presented by the authors in further papers.

3. Conclusion

The carried out push-out tests have shown the following results:

The load-carrying capacity of the studs is influenced by the slab bending moments. The influence depends on the ratio of reinforcement and the geometry of the sheets.

The transfer of stud shear forces in profiled concrete flanges can be described as a combination of the presented models based upon the truss-model theory.

4. Acknowledgement

The authors are grateful to the Deutsche Forschungsgemeinschaft for sponsoring the research work presented in this paper. Further thanks are given to the Holorib GmbH, Germany and the Solac Socie Social, France for the contribution of the profiled sheets and to TRW Nelson GmbH, Germany for the stud shear connectors.

5. References

[1] Bode, H., Künzel, R.: Zur Anwendung der Durchschweißtechnik im Verbundbau. Fachgebiet Stahlbau Universität Kaiserslautern, Forschungsbericht 1991.

[2] Bode, H, Künzel, R.: Zur Traglast von Verbundträgern unter besonderer Berücksichtigung einer nachgiebigen Verdübelung. Fachgebiet Stahlbau, Universität Kaiserslautern, Forschungsbericht 1988.

[3] Johnson, R. P., Huang, D.: Resistance to longitudinal shear of composite beams with profiled sheeting. Proc. Instn. Civil Engineers, Structurs and Biuldings, Vol. 110, May 1995, Pages 204 - 215.

[4] Lloyd, R. M., Wright, D.: Shear Connection between Composite Slabs and Steel beams. Journal Construction Steel Research No. 15, (1990), Pages 255 - 285.

[5] Ramm, W., Jenisch, F.-M.: Load-bearing behaviour of composite slabs as a part of composite beams. Engineering Foundation Conference, Composite Construction III, Irsee, Germany, June 1996.

[6] Ramm, W., Jenisch, F.-M.: Tragverhalten und Bemessung von Gurtplatten unter Schub und Querbiegung bei Verbundträgern und bei Verwendung von Profilblechen. Fachgebiet Massivbau und Baukonstruktion, Universität Kaiserslautern, Zwischenbericht 1993.

Interaction between Hollow Core Slabs and Supporting Beams

Matti PAJARI
Senior Research Scientist
VTT Building Technology
Espoo, Finland

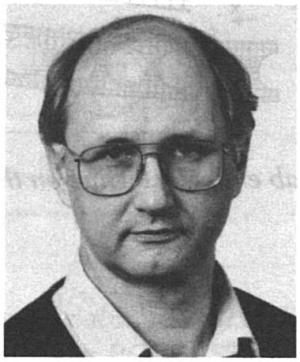

Matti Pajari, born 1948, received his DTech at Helsinki University of Technology in 1995. Since 1978, he has been involved in research and development projects concerning reinforced and prestressed concrete structures.

Summary

Ten full-scale loading tests on floors comprising prestressed hollow core slabs and steel, concrete or composite beams have been carried out. In every test the slabs underwent a web shear failure. In nine of these tests the observed shear resistance of the slabs was 40 to 74%, and in one test 98% of the shear resistance observed in reference tests. The reduction in the shear resistance can be explained by the shear interaction between the slabs and the beams. A simple calculation model to take account of this effect is presented.

1. Introduction

When loading a floor in which hollow core slabs are supported on beams, both the slabs and the beams deflect, cf. Fig. 1a. In such a floor the ends of slab units, especially those close to the columns, are subjected to both vertical and transverse shear (here transverse means the same as parallel to the beams) and deform as illutrated in Fig. 1b. This is called *shear interaction effect.* It may cause the webs of the slabs to fail under a vertical shear force considerably weaker than observed for a slab supported on a rigid bearing. The same effect occurs in other slab types, too. However, the effect is most important in prestressed hollow core slabs, because, due to the production technology, their thin webs cannot be provided with shear reinforcement.

The present paper briefly summarizes some results of ten full-scale load tests and design rules based on these results. A more comprehensive view is given by Pajari & Yang (1994), Pajari (1995, 1997), Pajari & Koukkari (1997), and Leskelä & Pajari (1995). To the author's knowledge, neither experimental nor theoretic research on this topic had been done before the first three of the present tests were performed. Since then, Leskelä has independently explained the test results of VTT, formulated theoretic and numeric calculation models and developed practical design methods (1991a,b, 1993, 1994). Borgogno & Fontana (1995) have carried out fire tests on PHC slabs supported on beams. In their tests the shear resistance of the slabs was not exceeded, which may be explained by the short slab spans (= 2.4 m), strengthening of the slabs and small loads.

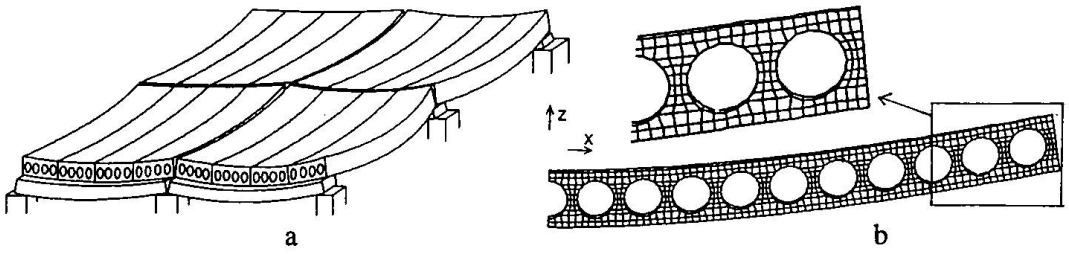

Fig. 1 a) Deformed PHC floor. b) Deformed slab end. Centerline on the left, longitudinal edge on the right

2. Test arrangements

Fig. 2 depicts the test layout and Fig. 3 the nominal slab cross-sections. Table 1 gives some characteristics of the tests.

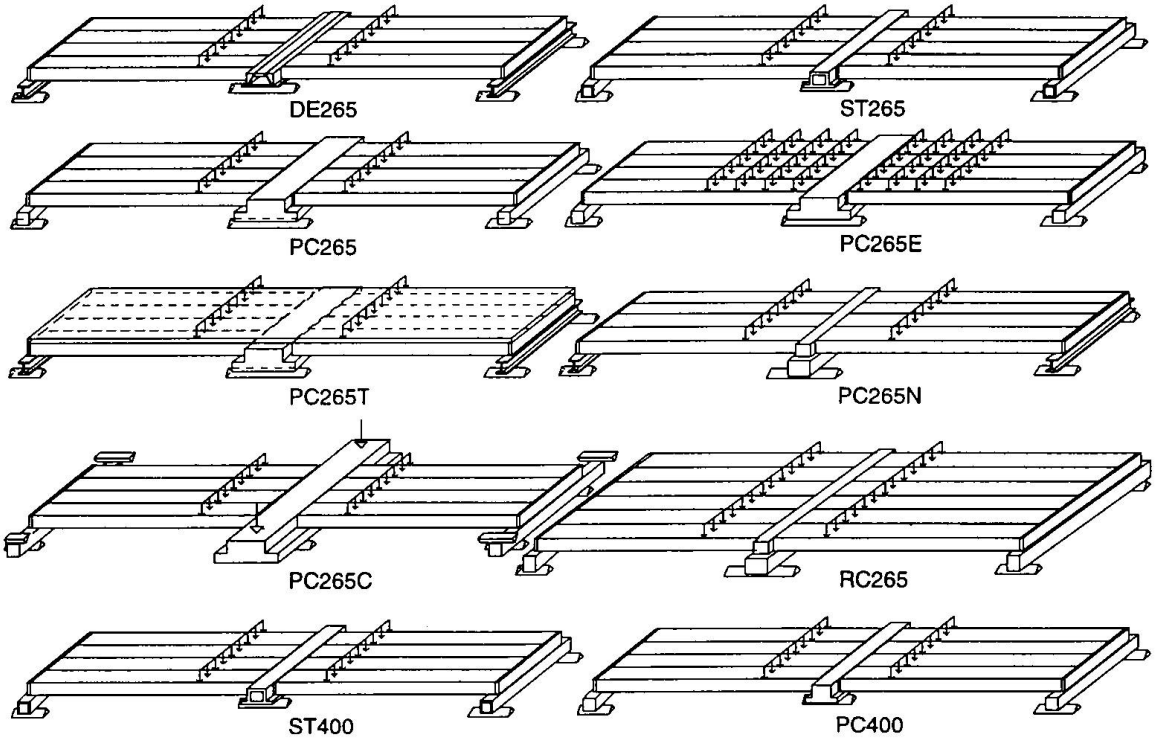

Fig. 2 Layout for floor tests

The test codes are of type XYABCZ, where XY refers to the middle beam (PC and RC for prestressed and reinforced concrete beam, respectively, ST for top-hat steel beam and DE for Delta beam which is a certain type of composite beam). ABC is the slab thickness in mm and Z an optional suffix (E refers to evenly (uniformly) distributed load, T to topping concrete, C to clamping of beams and N to normal beam which is positioned totally below the slabs).

Some of the tests were basic tests which aimed at simulating the behaviour of the floor when no special measures are taken; others clarified the effect of special measures like void filling or reinforced concrete topping. The loading arrangements were planned to exclude failure modes

other than the failure of the middle beam or shear failure of the slabs. The end beams were designed to undergo the same deflection as the middle beam.

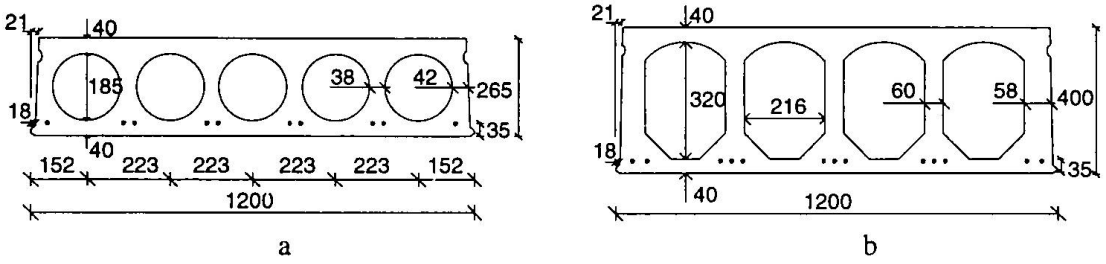

Fig. 3 Nominal cross-section of slabs. a) Tests DE265, ST265, PC265, PC265E, PC265T, PC265N, PC265C, RC265. b) Tests PC400, ST400

Table 1 Types of beam, slab length (L_{sl}), span of the middle beam (L_b) and distance of the line load(s) from the slab end a (a_i)

Test	Middle beam	End beam	L_{sl} mm	L_b mm	a (a_i) mm	Note
DE265	Delta	ST, I	6000	5000	1000	Composite beam
ST265	ST, top-hat	ST, box	6000	5000	1000	Basic test
PC265	PC, invert. T	RC, rectangle	6000	5000	1000	Basic test
PC265E	PC, invert. T	ST, I	6000	5000	375, 1125, 1875, 2625	Filled voids (185 mm) eight line loads
PC265T	PC, invert. T	ST, I	6000	5000	1000	RC topping
PC265N	PC, rectangle	ST, I	6000	5000	1000	Normal beam
PC265C	PC, invert. T	ST, I	6000	5000	1000	Beam with clamped ends
RC265	RC, rectangle	RC, rectangle	6000	7200	1200	Cracked normal beam
PC400	PC, invert. T	RC, rectangle	7200	5000	1260	Filled voids (320 mm)
ST400	ST, top-hat	ST, I	7200	5000	1260	Basic test

3. Test results

All tests ended with web shear failure of the slabs close to the middle beam. In test PC265C with clamped beams, all slab units failed simultaneously on one side of the middle beam. In other tests, the failure took place in one to four slab units close to the supports of the midlle beam. Table 2 gives the shear resistance observed in the floor test and in reference tests carried out on similar slab units supported on non-settling supports.

In nine tests, the observed shear resistance of the slabs was 40 to 75% of the resistance observed in the reference tests, and 98% in test PC265C with clamped beams. The measurements and analytical considerations showed that only in test PC265E was the middle beam yielding when the slabs failed. In other tests, the slabs were not capable of carrying a load corresponding to the resistance of the beams. This contradicts the conventional design methods according to which the failure should have been governed by the resistance of the beams, not by the resistance of the slabs. Therefore, the shear interaction effect must be taken into account when designing hollow core floors supported by beams.

Filling the voids and applying reinforced concrete topping proved to be effective, but they could not totally eliminate the reduction in the shear resistance of the slabs. Clamping the ends of the beams was still more effective: in test PC265C no reduction in shear resistance was observed.

The deflections of the middle beams were small, typically 1/800 to 1/300 of the span of the beam.

Table 2 Comparison of shear resistance observed in floor test (V_{obs}) with that observed in reference tests (V_{ref})and with the support reaction corresponding to the predicted resistance of the middle beam ($V_{sl,b}$) (no contribution from the slabs or joint concrete assumed)

Test	V_{obs} kN	V_{ref} kN	$\frac{V_{obs}}{V_{ref}}$	$V_{sl,b}$ kN	$\frac{V_{obs}}{V_{sl,b}}$
DE265	113.6	284.5	0.40	147.0	0.77
ST265	166.1	231.1	0.72	169.7	0.98
PC265	103.8	231.1*	0.45	116.6	0.89
PC265E	146.8	251.8	0.58	121.6	1.21
PC265T	142.8	193.3	0.74	135.0	1.06
PC265N	163.4	217.5	0.75	172.1	0.95
PC265C	191.7	194.9	0.98	191.8	1.00
RC265	106.8	226.2	0.47	78.0	1.37
PC400	255.4	483.0	0.53	312.5	0.82
ST400	293.9	516.3	0.57	308.6	0.95

* Value measured for slab units in test ST265

4. Analysis of web shear failure using composite beam model

Consider an infinitesimal cube taken from a web of a hollow core slab as shown in Fig. 4a.

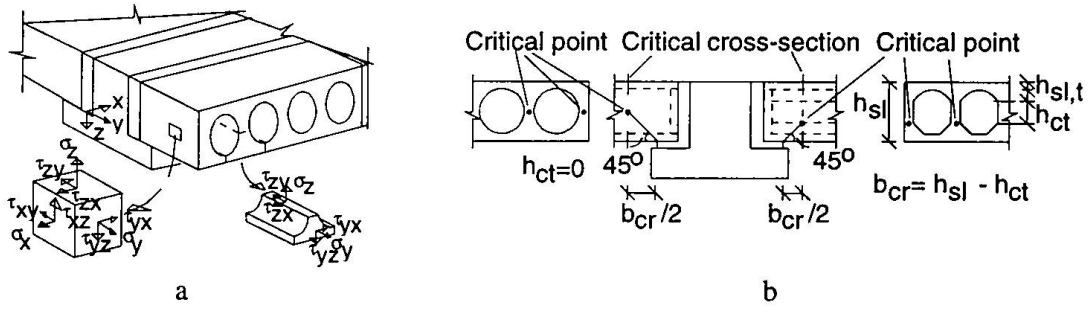

Fig. 4 Stress components in the web

The critical point may be assumed to be so far from the supporting beam that the local effect of the support reaction on the stress state may be ignored, i.e. the resultant of σ_z in a horizontal cross-section may be ignored. σ_x and τ_{xy} are obviously insignificant at the mid-depth of the web and may be ignored. σ_y and τ_{zy} can be calculated as in the conventional design of hollow core slabs. For reasons explained elsewhere (Pajari 1995), a failure criterion based on the interaction of the transverse and vertical shear in the webs of the slabs is adopted. The transverse shear flow v in the webs is calculated using the composite beam model shown in Fig. 5.

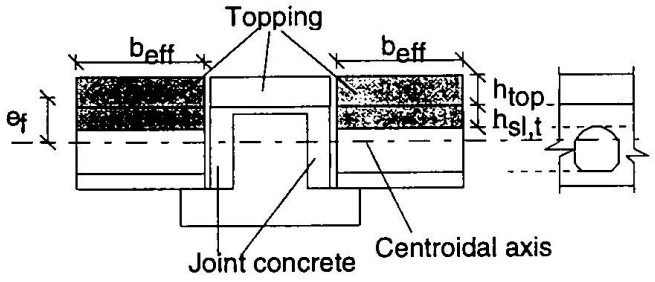

Fig. 5 Composite beam model

The value of effective width b_{eff} depends on the slab, beam and their interaction. By dividing v over a critical length b_{cr} defined in Fig. 4b, τ_{zy} is obtained. The adopted failure criterion is

$$f_{ct} = \frac{\sigma_y}{2} + \sqrt{\frac{\sigma_y^2}{4} + \tau_{zy}^2 + (\beta\tau_{zx})^2} \qquad (1)$$

where f_{ct} is the axial tensile strength of the concrete and β a reduction factor which takes into account extra measures like void filling, topping reinforcement etc. Both b_{eff} and β are determined experimentally. Table 3 gives recommended values of b_{eff} based on the tests.

Table 3 Effective width for floors similar to test floors

Beam	Slab mm	b_{eff} / L_b %
Concrete beam	265	3.72
	400	8.00
Steel beam	265	1.76
	400	2.30
Delta beam	265	2.74

As an example, consider how the span of the beam affects the resistance of the slabs when other parameters are constant (see Pajari 1995 for the structural data). For short spans the resistance of the slab is critical (Fig. 6). The resistance of the beam is critical for long spans. The arrow shows where the difference between the conventional and the proposed design criteria is greatest.

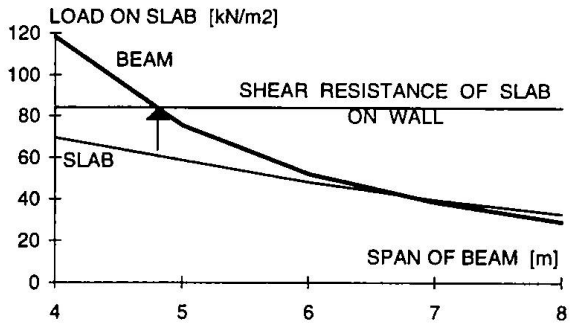

Fig. 6. Effect of span of beam on resistances of beam and slab.

5. Concluding remarks

According to the test results, the shear resistance of hollow core slabs may be considerably reduced due to the deflection of the supporting beams. Typical reductions in the tests were 25 - 60%. The amount of reduction depends on the interaction of the slabs and the beams.

It has been common practice to assume that the composite action, if present but not taken into account in the design, provides the structure with extra safety. Most of the tests showed opposite behaviour: the load-carrying capacity of the floor was lower than that corresponding to the resistances of isolated beams and slabs. The composite action transfers strain energy from the beams to the slabs, which gives rise to web shear failure in the slabs under a relatively low load. The shear resistance can be enhanced by filling the voids of the slabs at their ends, by using reinforced concrete topping, by making the beams stiffer or continuous etc. However, the reduction of shear resistance cannot be ignored in the design of hollow core slabs supported on beams. A simple, semiempiric calculation model is presented. It is currently being used in Finland, Sweden and in The Netherlands.

References

Borgogno, W. & Fontana, M. (1995). "Brandverhalten von Slim-Floor-Verbunddecken (Fire Behavior of Slim-Floor composite floors)." *Stahlbau,* Germany, 64, Heft 6, 168-174.

Leskelä, M.V. (1991a). "Strength Reduction in Hollow-Core Slabs when Supported by Beams and Girders." Norske Betongforening, *Nordic Concrete Research,* Public. No. 10, Oslo, 16 p.

Leskelä, M.V. (1991b). "The Shear Failure Condition in Hollow-Core Slab Units Loaded by Vertical and Transverse Shear Force Components." *Journal of Structural Mechanics,* Vol. 24, No. 2, Espoo, Finland, 22 - 29.

Leskelä, M.V. (1993). "Slim-Floor Beams: Design Criteria and Structural Behaviour." *Proc., The Engineer. Found. Confer. Composite Construction II*, Potosi, Missouri, ASCE, 182 - 197.

Leskelä, M.V. (1994). Shear Flow Calculations for Slim-Type Composite Beams Supporting Hollow-Core Slabs." *Proc., The Fourth International Conference: Steel-Concrete Composite Structures*, Bratislava, ACCS, 299-302.

Leskelä, M.V. & Pajari, M. (1995). "Reduction of the Vertical Shear Resistance in Hollow-Core Slabs when Supported on Beams." *Proc., Concrete 95 Conference,* Vol. 1, Brisbane, 559 - 568.

Pajari, M. & Yang, L. (1994). "*Shear Capacity of Hollow Core Slabs on Flexible Supports.*" Technical Research Centre of Finland, Espoo, VTT Research Notes 1587, 111 p + app. 26 p.

Pajari, M. (1995a). "Shear Resistance of Prestressed Hollow Core Slabs on Flexible Supports." Technical Research Centre of Finland, Espoo, VTT Publications 228, 132 p + app. 25 p.

Pajari, M. & Koukkari, H. "Shear Resistance of Prestressed Hollow Core Slabs Supported on Beams: Part I." Submitted for publication to ASCE, December 1996.

Pajari, M. "Shear Resistance of Prestressed Hollow Core Slabs Supported on Beams: Part II." Submitted for publication to ASCE, December 1996.